

A Method of Light Reflectance Measurement

by

Lun Ke

B.Sc.(Computer Science) Tsinghua University, 1993

A THESIS SUBMITTED IN PARTIAL FULFILLMENT OF

THE REQUIREMENTS FOR THE DEGREE OF

MASTER OF SCIENCE

in

THE FACULTY OF GRADUATE STUDIES

(Department of Computer Science)

We accept this thesis as confirming

to the required standard

.....

.....

THE UNIVERSITY OF BRITISH COLUMBIA

April 1999

© Lun Ke, 1999

In presenting this thesis in partial fulfillment of the requirements for an advanced degree at the University of British Columbia, I agree that the Library shall make it freely available for reference and study. I further agree that permission for extensive copying of this thesis for scholarly purposes may be granted by the head of my department or by his or her representatives. It is understood that copying or publication of this thesis for financial gain shall not be allowed without my written permission.

Computer Science

The University of British Columbia

2366 Main Mall

Vancouver, BC

Canada V6T 1Z4

Date: _____

Abstract

The quality of light reflectance models in realistic image synthesis is directly related to the quality of computer generated images. In order to develop such models, actual light reflectance distribution data are required. One way to express the reflectance properties of a surface is called *bidirectional reflectance distribution function*, or BRDF. BRDF is a function with four degrees of freedom, two for the direction of incident light and two for the direction of reflected light. It requires acquiring large amount of data through measurements and the process is very time consuming.

In this thesis, an automated measurement method is presented and implemented. A 3-channel CCD camera is calibrated and used as the light measuring device. The system used is called ACME (ACTIVE Measurement Facilities). Within ACME, all devices in the system are under robotics control. Experiments are written in Java, and can be loaded from any machine via Internet and run on the local server.

Several material samples are measured by using this system including paper and silk, and reliable data were obtained. The overall error is estimated to be less than 8%. It can be concluded that a CCD camera can be used to measure light reflectance properties for computer graphics, and it is relatively fast and convenient.

Table of Contents

Abstract	ii
List of Tables	vi
List of Figures	vii
Acknowledgments	x
Chapter 1 Introduction	1
1.1 The Bidirectional Reflectance Distribution Function	1
1.2 BRDF Measurement	4
1.3 Thesis Organization	5
Chapter 2 Related Work	6
2.1 Murray-Coleman’s directional reflectometer	6
2.2 Ward’s silver hemisphere reflectometer	8
2.3 Measurement method at Columbia University	10
2.4 The Gonioreflectometer at Cornell University	12
2.5 Comments on Previous Works	14
Chapter 3 System Description	16
3.1 Equipment Description	16
3.1.1 CCD Camera	16
3.1.2 Gantry.....	17
3.1.3 Test Station.....	17
3.1.4 Light Source	17
3.1.5 Radiometer	17
3.1.6 Equipment Integration.....	18
3.2 Software Structure	19

Chapter 4 Camera Calibration	22
4.1 Basic Principles of CCD Camera	22
4.2 CCD Camera Calibration.....	23
4.2.1 Calibration for Source Radiance	24
4.2.2 Calibration for Exposure Time.....	25
4.2.3 Calibration for F-number	26
4.3 Standard Pixel Value and Irradiance.....	27
Chapter 5 Data Acquisition and Treatment.....	29
5.1 Size of Test Sample	29
5.2 Data Acquisition Steps	29
5.3 Image Post Processing	31
5.3.1 Locating the Sample in the Image.....	32
5.3.2 Converting to Standard Pixel Value	34
5.3.3 Converting to Radiance Value.....	35
Chapter 6 Results and Analysis.....	37
6.1 Isotropic Check	37
6.2 Bidirectional Reflectance	41
6.2.1 Sample 1: Plain Paper	41
6.2.2 Sample 2: Silk	45
6.3 Error Analysis	50
Chapter 7 Conclusion and Future Work.....	52
7.1 Conclusion	52
7.2 Future Work	52
7.2.1 Improvement of Accuracy	52
7.2.2 Automating the Whole Process.....	53
7.2.3 BRDF Verification.....	53
Bibliography	55

Appendix A Light Measurement Basics	58
A.1 Light Basics.....	58
A.2 Measurement Principles.....	59
A.2.1 The Inverse Square Law	59
A.2.2 Lambert’s Cosine Law	59
A.3 Related Units.....	60
Appendix B Operating Procedures and Precautions	62
B.1 Camera Calibration	62
B.2 Experiment Process.....	63
B.2.1 Hardware Side	63
B.2.2 Software Side.....	63
Appendix C Resources and their locations	65

List of Tables

Table 1.1 Units of light measurement	3
Table A.1 Radiometric quantities.....	60

List of Figures

Figure 1.1 Reflection geometry	2
Figure 2.1 A gonioreflectometer designed by Murray-Coleman and Smith (copied from[Murray90])	6
Figure 2.2 Free variables in Murray’s gonioreflectometer	7
Figure 2.3 Ward’s silver hemisphere reflectometer (copied from [Ward92]).....	8
Figure 2.4 Half-silvered hemisphere geometry of Ward’s gonioreflectometer (copied from [Ward92]).....	9
Figure 2.5 Free variables in Ward’s gonioreflectometer.....	9
Figure 2.6 The BRDF measuring equipment in Columbia University (copied from [Dana96]).....	10
Figure 2.7 Sample orientations (copied from [Dana96]).....	11
Figure 2.8 Free variables in the gonioreflectometer at Columbia University	12
Figure 2.9 Gonioreflectometer at Cornell Light Measurement Laboratory (copied from [Sing97]).....	13
Figure 2.10 Overhead view of the gonioreflectometer at Cornell (copied from [Sing97])	13
Figure 2.11 Free variables in the gonioreflectometer at Cornell	14
Figure 3.1 Light Source Structure	18
Figure 3.2 System connection Diagram	18
Figure 3.3 ACME system	19
Figure 3.4 ACME software design.....	20
Figure 3.5 The structure of ACME packages	21
Figure 4.1 Spectral quantum efficiency curve of Sony DCX950 CCD camera (supplied by manufacturer).....	23
Figure 4.2 Pixel value as a function of radiometer reading.....	24

Figure 4.3 Image forming system.....	25
Figure 4.4 Pixel value as a function of exposure time.....	26
Figure 4.5 Pixel value as a function of the 4-th power of camera f-number	27
Figure 5.1 Devices when sample and light are attached to test station	30
Figure 5.2 An image captured by CCD camera.....	32
Figure 6.1 Isotropic check of white paper with incident angle of 65° and view angle of 50° ..	38
Figure 6.2 Isotropic check of white paper with incident angle of 65° and view angle of 80° ..	38
Figure 6.3 Isotropic check of white paper with incident angle of 45° and view angle of 50° ..	39
Figure 6.4 Isotropic check of white paper with incident angle of 45° and view angle of 80° ..	39
Figure 6.5 Isotropic check of red silk with incident angle of 65° and view angle of 50°	40
Figure 6.6 Isotropic check of red silk with incident angle of 65° and view angle of 80°	40
Figure 6.7 Isotropic check of red silk with incident angle of 45° and view angle of 50°	41
Figure 6.8 Isotropic check of red silk with incident angle of 45° and view angle of 80°	41
Figure 6.9 Side view of white paper's BRDFs with the incident direction at 65° to the right	42
Figure 6.10 Overhead view of white paper's BRDFs with the incident direction at 65° to the right.....	43
Figure 6.11 The incident plane of white paper's BRDFs with the incident direction at 65° to the right.....	43
Figure 6.12 Side view of white paper's BRDFs with the incident direction at 45° to the right.....	44
Figure 6.13 Overhead view of white paper's BRDFs with the incident direction at 45° to the right.....	44
Figure 6.14 The incident plane of white paper's BRDFs with the incident direction at 45° to the right.....	45
Figure 6.15 Side view of red silk's BRDFs with the incident direction at $(180^\circ, 65^\circ)$	46
Figure 6.16 Overhead view of red silk's BRDFs with the incident direction at $(180^\circ, 65^\circ)$	46
Figure 6.17 The incident plane of red silk's BRDFs with the incident direction at $(180^\circ, 65^\circ)$	47
Figure 6.18 Side view of red silk's BRDFs with the incident direction at $(180^\circ, 45^\circ)$	47
Figure 6.19 Overhead view of red silk's BRDFs with the incident direction at $(180^\circ, 45^\circ)$	48
Figure 6.20 The incident plane of red silk's BRDFs with the incident direction at $(180^\circ, 45^\circ)$	48

Figure 6.21 Side view of red silk's BRDFs with the incident direction at $(90^\circ, 65^\circ)$	49
Figure 6.22 Overhead view of red silk's BRDFs with the incident direction at $(90^\circ, 65^\circ)$	49
Figure 6.23 The incident plane of red silk's BRDFs with the incident direction at $(90^\circ, 65^\circ)$.	50
Figure A.1 The optical portion of the electromagnetic spectrum (copied from [LMH])	58
Figure A.2 CIE spectral tristimulus curve (copied from [Fournier96])	59
Figure A.3 Lambert's cosine law	60
Figure A.4 Steradian, unit of solid angle.....	61

Acknowledgments

First of all, I would like to thank my supervisor Dr. Alain Fournier for his advice and help on my thesis over the last two years. Alain has been always nice and patient when I need his help and advice. I learned a lot from his way of looking at the world, his way of thinking and etc.

I would also like to give thanks to Dr. Dinesh K. Pai, the project leader of ACME and my thesis' second reader, for his help on organizing all the facilities for the experiment and for his time on reading my thesis.

Special thanks go to Dr. Bob Woodham for providing the light source and the radiometer in the experiment. My thesis could not have been done without these facilities.

Thanks also go to Jochen Lang, Chris Chiu, Rod Barman, Stewart Kingdon and all the group members of ACME. They are kind and helpful, and always around when I need help. I learned a lot from them on how to operate various equipments in the LCI lab and how to deal with hardware problems.

Lun Ke

The University of British Columbia

April 1999

Chapter 1

Introduction

The goal of realistic image synthesis is to produce computer generated images that are indistinguishable from real scenes. The process begins with a scene definition, which includes the geometric description, the surface reflectance properties of objects and the description of light sources, and proceeds with determination of the visibility and light reflected by the visible surfaces towards the virtual camera. Most of these models are based on simulating the physical light transport. Early models consider either only ideal (perfect mirror) reflection, or diffuse reflection [Phon75]. Many recent light models have been presented to consider more complex light reflection [Blin77][Cook82][Poul90][He91], but more specific ones are based on physically measured light distribution data.

To achieve high quality in realistic computer generated image synthesis, a specific reflectance model should be based on and verified by measurements and experiments. In order to develop such a model, actual light reflectance distribution data are needed. One way to represent the reflectance property of a surface is named bidirectional reflectance distribution function, or BRDF [Cohen93]. This thesis is focused on a method to measure BRDF, and the measurement results of several material samples are also included.

1.1 The Bidirectional Reflectance Distribution Function

The bidirectional reflectance distribution function is an expression of the physical property of a material which describes the pattern of light reflected from a surface of the material to all directions above the surface, for all directions of incident light. It is a four-dimen-

sional function if we leave wavelength out of consideration. For a homogeneous surface, the BRDF determines the appearance of materials for different viewing directions.

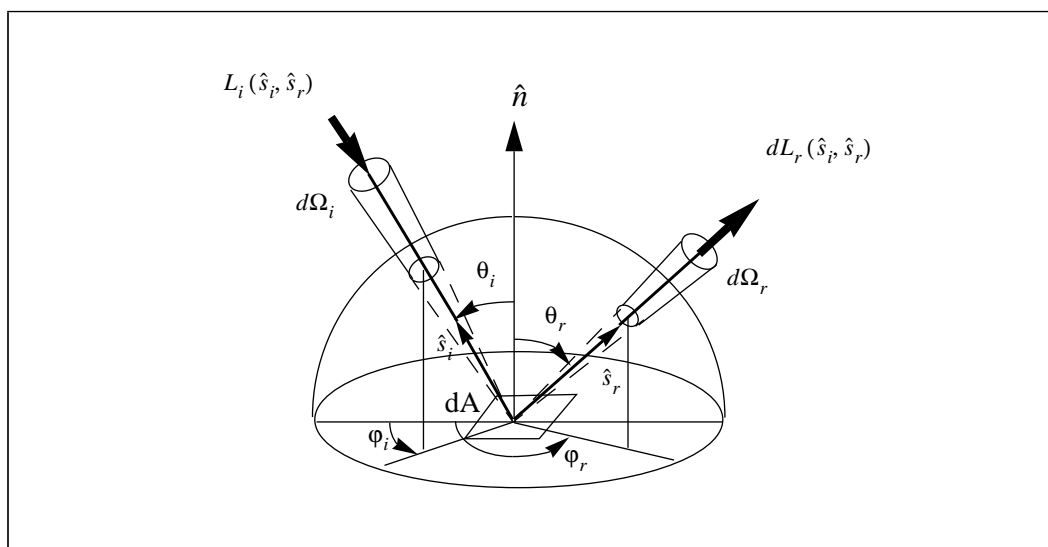


Figure 1.1 Reflection geometry

The geometry of bidirectional reflection process is shown in Figure 1.1. A surface is shown illuminated from a direction (θ_i, ϕ_i) by a radiation centered within a solid angle $d\Omega_i$ with reflection in the direction (θ_r, ϕ_r) , centered within a cone $d\Omega_r$. The bidirectional reflectance distribution function (BRDF) is defined as the ratio of the directional reflected *radiance* to the directional incident *irradiance* (see Appendix A). *Radiance* is the radiant power flow per unit solid angle and unit area normal to the rays and has the unit $[\text{Wm}^{-2}\text{sr}^{-1}]$. *Spectral radiance* is the radiance per unit wavelength and has the unit $[\text{Wm}^{-3}\text{sr}^{-1}]$. *Irradiance* is the power flux density irradiating a surface per unit area of the surface and has unit $[\text{Wm}^{-2}]$. For the cone-surface geometry in Figure 1.1, the area normal to the ray is calculated as $\cos\theta_r dA$ for the cone of reflection and $\cos\theta_i dA$ for the cone of incidence. Spectral irradiance is the incident irradiance expressed in per-unit wavelength with unit $[\text{Wm}^{-3}]$. Table 1.1 gives a summary of these units.

Table 1.1 Units of light measurement

Symbol	Name	Unit
L_i, L_r	radiance	$Wm^{-2}sr^{-1}$
E_i, E_r	irradiance	Wm^{-2}
$L_{\lambda i}, L_{\lambda r}$	Spectral radiance	$Wm^{-3}sr^{-1}$
f_r	BRDF	sr^{-1}

In terms of the foregoing quantities, the BRDF is defined as a function of wavelength in [Modest93]¹:

$$f_r(\lambda, \hat{s}_i, \hat{s}_r) = \frac{dL_{\lambda, r}(\lambda, \hat{s}_i, \hat{s}_r)}{dE_{\lambda, i}(\lambda, \hat{s}_i)} \quad (\text{Eqn 1-1})$$

where $dE_{\lambda, i}$ is the incident spectral irradiance, and $dL_{\lambda, r}$ is the reflected spectral radiance. Note that the BRDF is reciprocal in general [Modest93]. If the incident and reflected directions are reversed, the function has the same value. Further, the radiance does not vary along the direction of propagation of a ray, in the absence of out-scattering or in-scattering along the ray. This will allow us to measure the reflected radiance at any distance from the reflecting surface, although some other rules need to be considered according to the experimental conditions (see section 1.2).

In most BRDF measurements for global illumination, wavelength and polarization notation are omitted. After the wavelength is dropped, the BRDF becomes:

$$f_r(\hat{s}_i, \hat{s}_r) = \frac{dL_r(\hat{s}_i, \hat{s}_r)}{dE_i(\hat{s}_i)} \quad (\text{Eqn 1-2})$$

where, at any particular wavelength λ_0 , it is understood that the radiance is

1. For some material with internal scattering, the reflected light can come from a point different from the incident point. The BRDF expression given here ignores this.

$L_r \approx L_{\lambda, r}(\lambda_0, \hat{s}_i, \hat{s}_r) \Delta\lambda$ and the irradiance is $E_i \approx E_{\lambda, i}(\lambda_0, \hat{s}_i) \Delta\lambda$, where $\Delta\lambda$ is a finite bandwidth of wavelength.

With $d\Omega_i$ as the incident solid angle, the irradiance dE_i may be expressed in term of an incident radiance L_i as

$$dE_i(\hat{s}_i) = \cos\theta_i L_i(\hat{s}_i) d\Omega_i \quad (\text{Eqn 1-3})$$

The cosine term serves to project the surface area in the incident direction \hat{s}_i . Note that the incident radiance L_i is not a differential, but a finite quantity. (Eqn 1-3) actually states the *cosine law* of light measurement. For more information about *cosine law*, refer to Appendix A.

1.2 BRDF Measurement

BRDF is difficult to measure, since it is a function with four degrees of freedom even if the wavelength is ignored. It also requires large data storage, because for each incident direction the intensity of reflectance in all directions should be measured and stored. For these reasons, most computer graphics labs do not measure the data themselves. There are a few professional labs in North America where one can send a surface sample for BRDF characterization [Ward92], but it is costly. To get the essential data for BRDF within an affordable budget is desirable for graphics people, since the range of materials they want to measure might be very large.

A device for measuring BRDF is called a gonireflectometer (*gonio* is borrowed from the Greek, meaning “angle”). The usual design for such a device includes a light source, a sample area that can be moved in relation to the light source and a photometer that can be moved in relation to the sample area. Because the BRDF is a function of four angles, such a device must have at least four degrees of mechanical freedom to measure the complete function.

In this thesis, BRDF measurement is accomplished by employing ACME facilities.

ACME, the Active Measurement Facility, is an integrated robotic facility designed to acquire rich measurements for the purpose of building accurate computational models. ACME facility is located in the Laboratory of Computational Intelligence (LCI) of the Computer Science Department, University of British Columbia. The latest information about ACME can be found at <http://www.cs.ubc.ca/nest/lci/acme/>

1.3 Thesis Organization

The rest of the thesis is organized as follows. Chapter 2 gives a brief review of BRDF measurement systems built in other graphics labs. Chapter 3 describes our measurement system, including both hardware and software environments. Chapter 4 gives the calibration results for the CCD camera we used to measure BRDFs. Chapter 5 describes the data acquisition and treatment process. Chapter 6 presents the measurement results for several samples. Conclusions are drawn and extensions for this work are proposed in Chapter 7.

Chapter 2

Related Work

Since it is essential to have the BRDF data for realistic image synthesis, several graphics labs built their own experimental devices. They will be briefly described in this chapter.

2.1 Murray-Coleman's directional reflectometer

An early and basic gonioreflectometer designed by Murry-Coleman and Smith [Murray90] is shown in Figure 2.1.

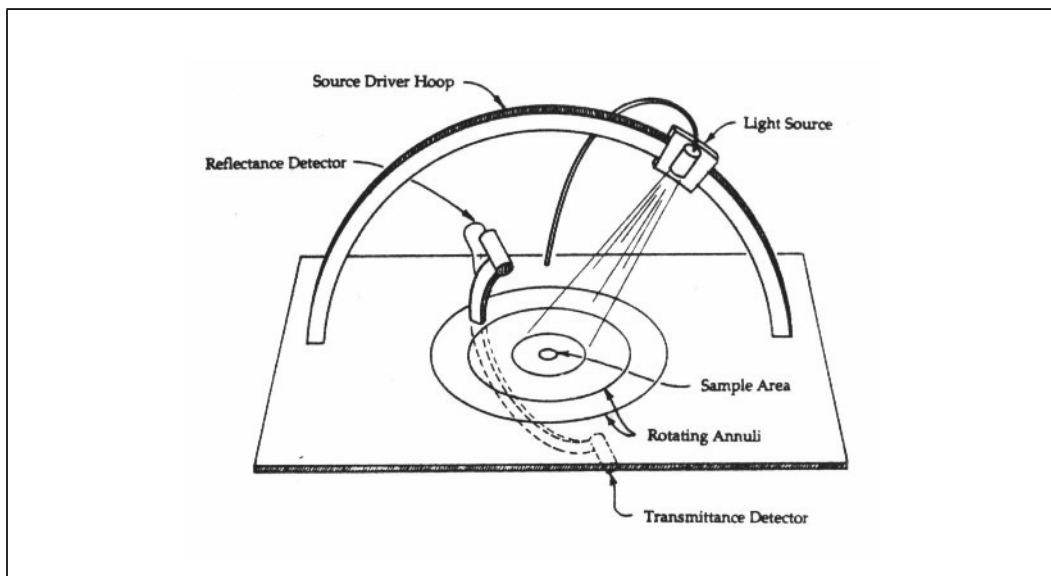


Figure 2.1 A gonioreflectometer designed by Murray-Coleman and Smith (copied from[Murray90])

In this system, the source, the detector and the sample are all positioned with stepper

motors that are controlled by a computer via standard RS232 serial port. The system provides four degrees of freedom, as required by the definition of the BRDF.

The light source used to illuminate the sample is an MR16 incandescent lamp, which is located below the sample platform. By using a fiber-optic light guide to bring the light flux from the lamp to the motorized carriage that contains the fiber optic end, the light source can remain fixed, permitting the lamp to have a fixed orientation throughout a measurement session. The luminance of the light source can be adjusted according to the reflectance of the sample to avoid overflow in the detector.

The photodetectors are of the silicon photodiode type. The optical arrangement of lens and aperture restricts the field of view of the detector to the sample and nearby area only. The samples are 6.5mm in diameter.

The data acquisition system measures a voltage differential proportional to the illuminance on the face of the photocell. After linear amplification of the photodetector output, an analog-to-digital conversion is performed, producing a 16-bit number proportional to the analog output of the photodetector.

Figure 2.2 shows the use of free variables in Murray's gonioreflectometer. In all such

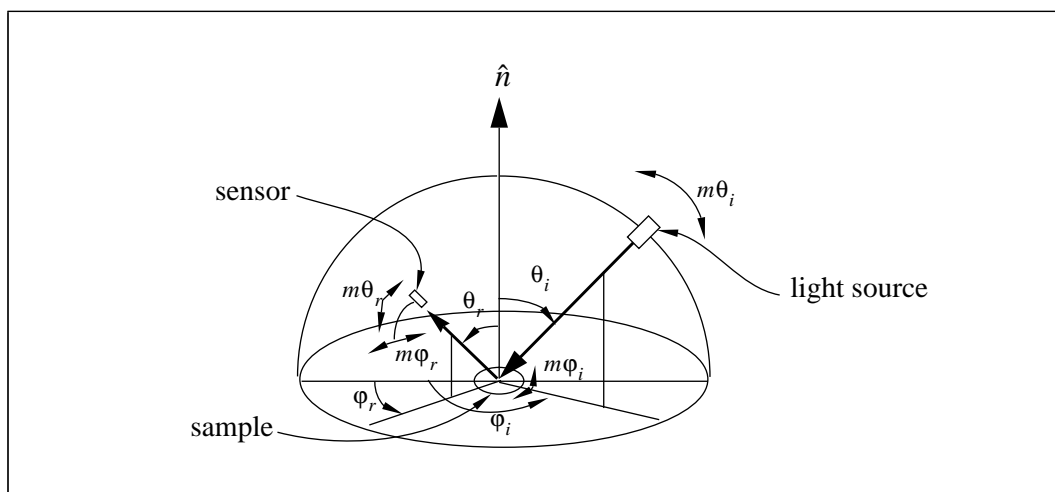


Figure 2.2 Free variables in Murray's gonioreflectometer

diagrams, $m\theta_i$ stands for motion that changes θ_i , $m\phi_i$ stands for motion that changes ϕ_i , $m\theta_r$ stands for motion that changes θ_r , and $m\phi_r$ stands for motion that changes ϕ_r .

2.2 Ward's silver hemisphere reflectometer

Gregory J. Ward [Ward92] in Lawrence Berkeley Laboratory developed a relatively simple device for measuring BRDFs that uses imaging technology. The basic arrangement of the imaging gonioreflectometer is shown in Figure 2.3.

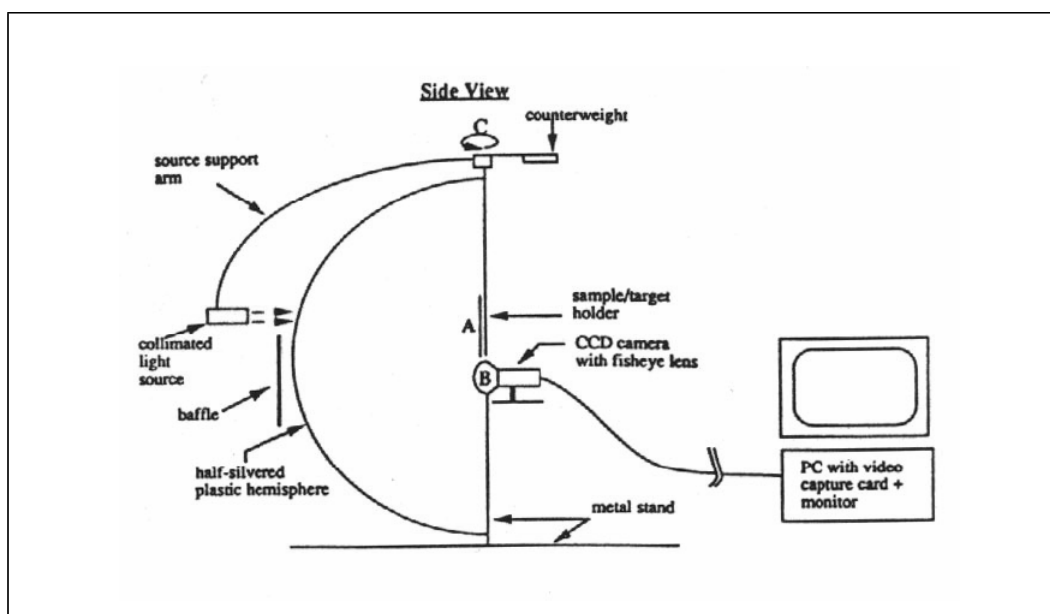


Figure 2.3 Ward's silver hemisphere reflectometer (copied from [Ward92])

The key optical elements are a half-silvered hemisphere and a CCD camera with a fish-eye lens. The combination of these elements takes care of the two degrees of freedom handled by a mechanically controlled photometer in Murray's gonioreflectometer. Light reflected off the sample surface in holder A is collected by the hemispherical mirror and reflected back into the fish-eye lens and onto the CCD array B. Figure 2.4 illustrates the advantage of using a half-silvered hemisphere. By focusing the lens at one half of the hemisphere radius, an image of luminance in all different reflected angles takes place.

The light source is a 3-watt quartz-halogen lamp. An optical precise parabolic reflec-

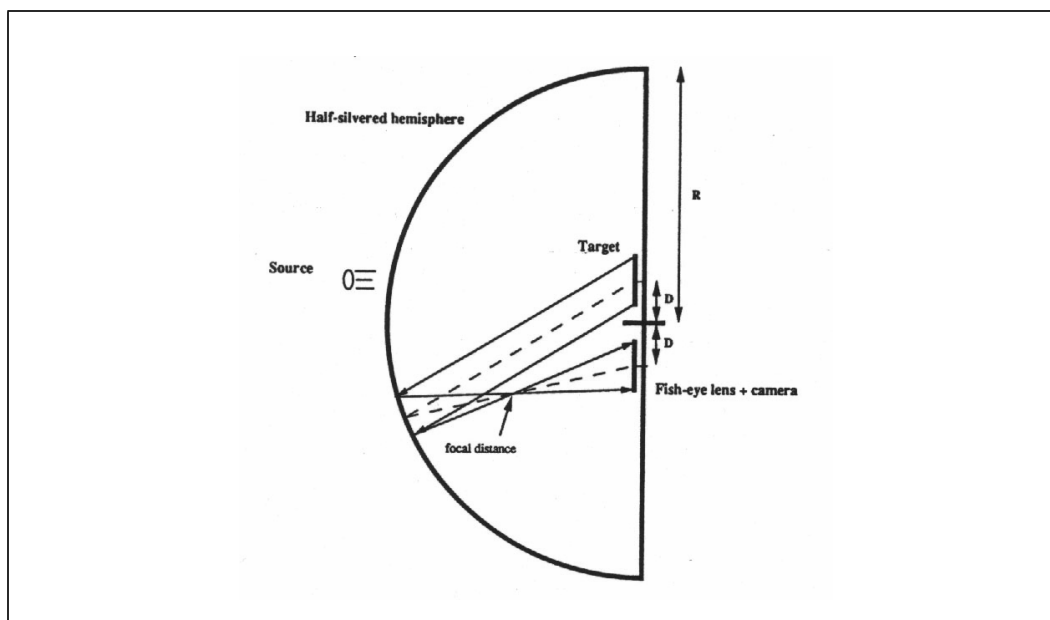


Figure 2.4 Half-silvered hemisphere geometry of Ward's gonioreflectometer (copied from [Ward92])

tor is used to produce a parallel beam. The hemisphere is half-silvered to allow the light beam to pass through and illuminate the sample, and an exterior baffle shields the camera from stray radiation.

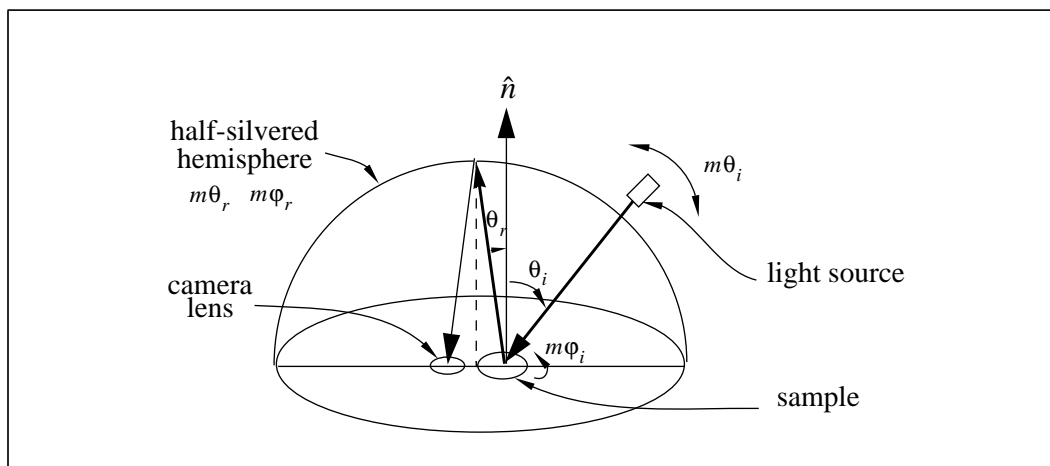


Figure 2.5 Free variables in Ward's gonioreflectometer

In Ward's system, the incident angles θ_i and ϕ_i are controlled mechanically by pivoting the light source arm at point C and the sample holder at point A, respectively (see Figure 2.3).

The light source is moved by a computer controlled motor during data collection, and the sample is moved manually. Figure 2.5 shows the system's free variables. Note that $m\phi_i$ is changed manually.

The prominent merit of Ward's device is that the hemisphere of reflection is captured in a single image, which makes data collection proceed quite rapidly. According to Ward's description, a complete BRDF measurement can be recorded in a few minutes, including time for manual rotation of the sample.

2.3 Measurement method at Columbia University

The Columbia Automated Vision Environment research group uses a robotic manipulator and a CCD camera to allow simultaneous measurement of BRDF and BTF (Bidirectional Texture Function) [Dana96]. The measurement equipment is depicted in Figure 2.6. It consists of a personal computer with a 24-bit RGB frame grabber, a robot arm to orient the samples, a halogen bulb with a Fresnel lens which produces a parallel beam, a spectrometer and a 3-channel CCD color video camera (not shown in Figure 2.6).

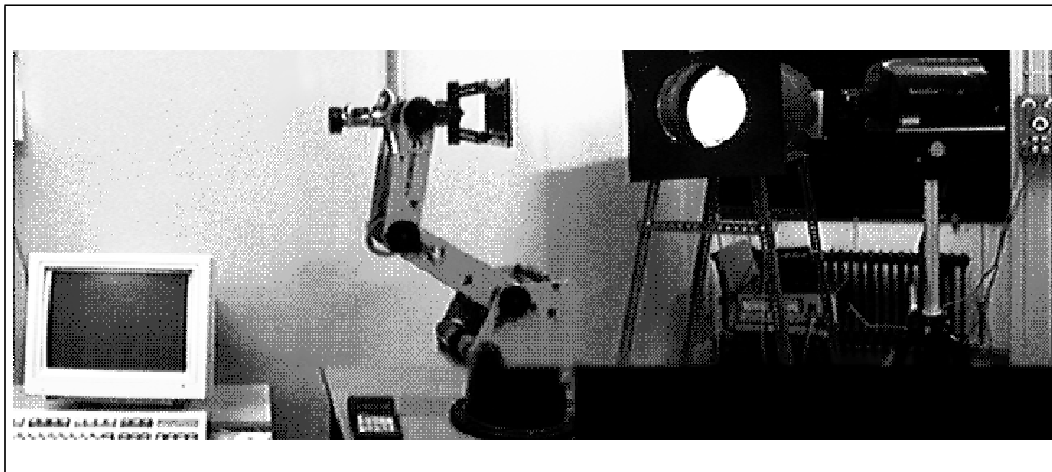


Figure 2.6 The BRDF measuring equipment in Columbia University (copied from [Dana96])

The light source remains fixed throughout the measurements. The light rays incident on the sample are approximately parallel and uniformly illuminates the sample. The camera is

mounted on a tripod and its optical axis is parallel to the floor of the lab. During the measurements for a given sample, the camera is moved to seven different locations, each separated by 22.5 degrees in the ground plane at a distance of 200 cm from the sample. For each camera position, the sample is oriented so that its normal is directed toward the vertices on the hemisphere, as illustrated in Figure 2.7.

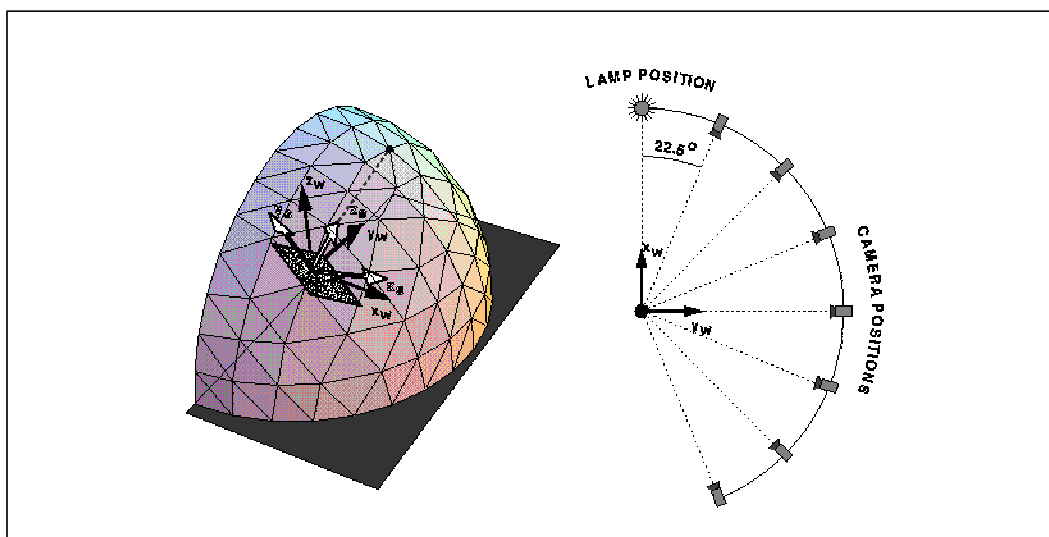


Figure 2.7 Sample orientations (copied from [Dana96])

The system's free variables are shown in Figure 2.8. Note the change of ϕ_r is done by changing the camera's position manually. The main constraint of this system is that when the robot arm moves, both the incident angle and reflection angle are changed. This makes it impossible to keep the incident angle fixed during a BRDF scan.

With this arrangement, a considerable number of measurements are made in the plane of incidence (i.e. the plane in which source direction, viewing direction and sample normal lie). Sample orientations with corresponding viewing angles or illumination angles greater than 85 degrees are excluded from the measurements to avoid self-occlusion and self-shadowing. This exclusion results in a collection of 205 images for each sample.

A BRDF and BTF database was established by using this equipment. Samples of these surfaces are 10x12 cm each. The database contains a collection of 61 real-world surfaces,

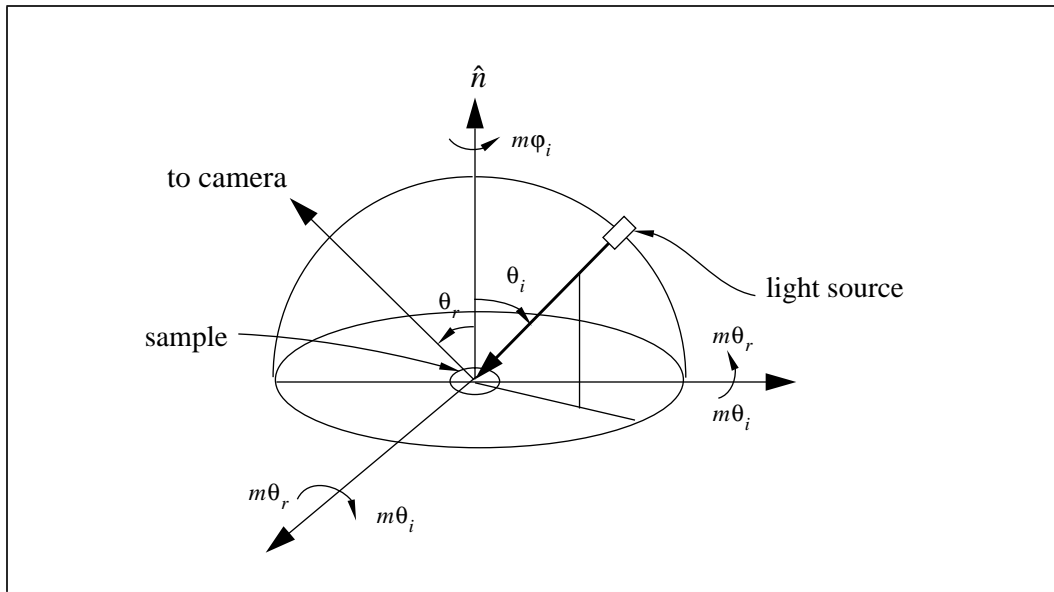


Figure 2.8 Free variables in the gonioreflectometer at Columbia University

including specular surfaces, diffuse surfaces, isotropic surfaces, anisotropic surfaces, etc. The database is available at <http://www.cs.columbia.edu/CAVE/curet>.

2.4 The Gonioreflectometer at Cornell University

The Light Measurement Laboratory at the Cornell University set up a gonioreflectometer to acquire reflection and emission data. Figure 2.9 gives a picture of the system and Figure 2.10 shows an overhead view of it.

In Figure 2.9, the device on the left is an optical detector, and the one on the right is a light source. The white area in the middle is a sample illuminated by the source. A folding mirror is used to lead the reflected light into the detector.

The sample mount pad has three degrees of freedom, both motion on a vertical plane and rotation. The light source has one degree of freedom, which is rotation around the sample. The system's free variable diagram is shown in Figure 2.11.

Although the whole system has four degrees of freedom altogether, it can only measure isotropic materials. Because of the way the stages are mounted, reflection angles are

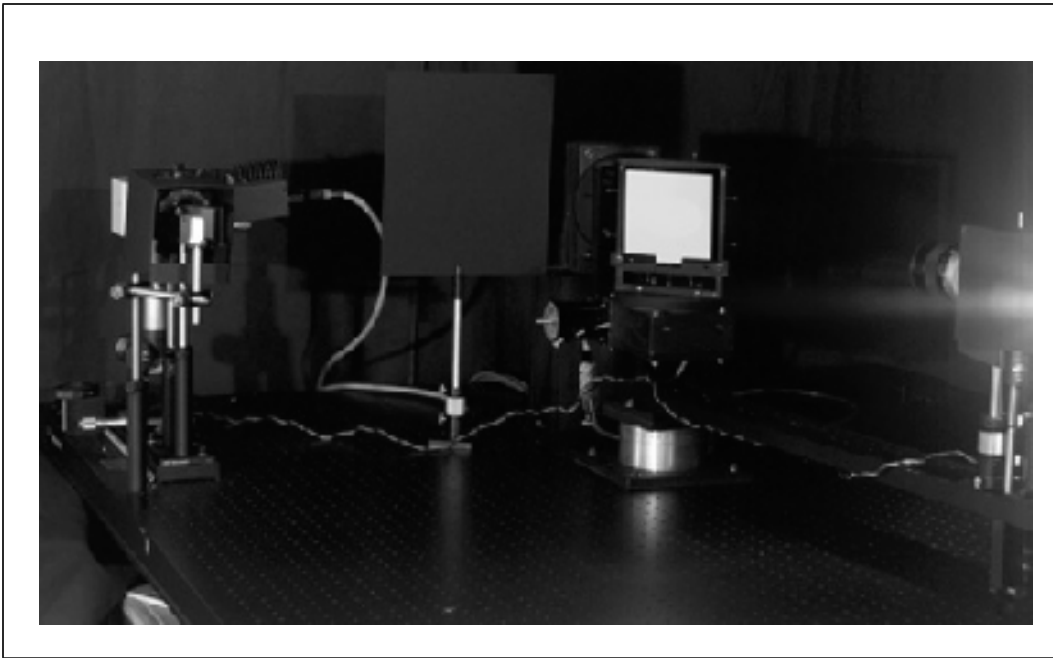


Figure 2.9 Gonioreflectometer at Cornell Light Measurement Laboratory (copied from [Sing97])

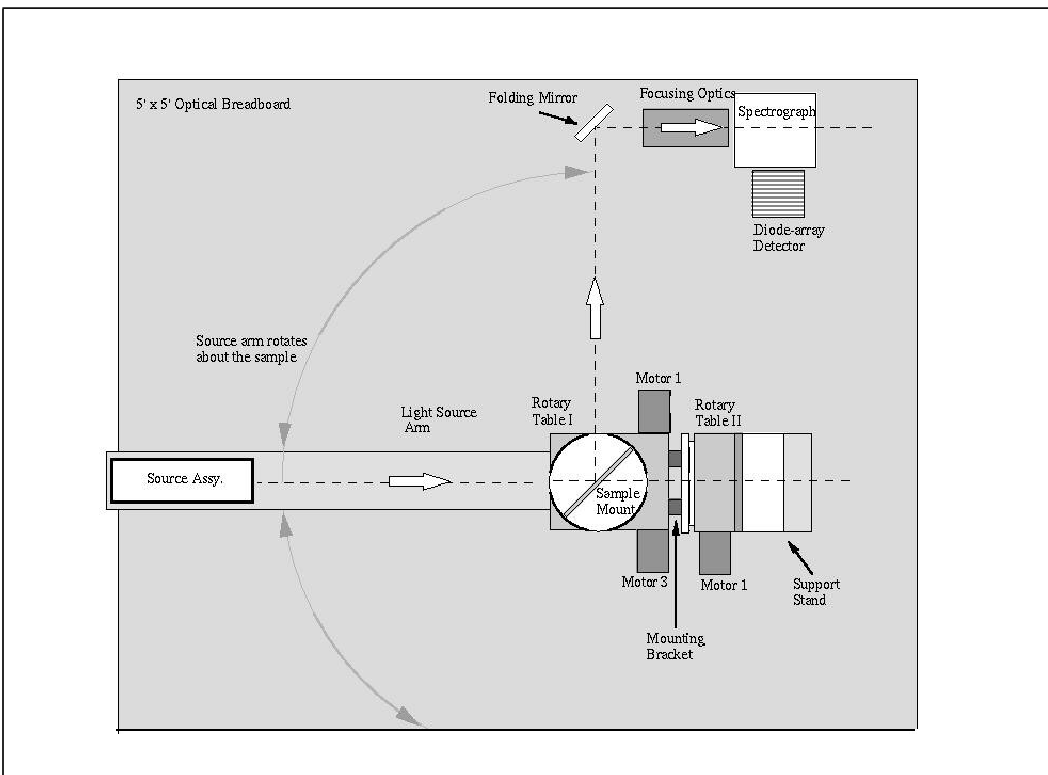


Figure 2.10 Overhead view of the gonioreflectometer at Cornell (copied from [Sing97])

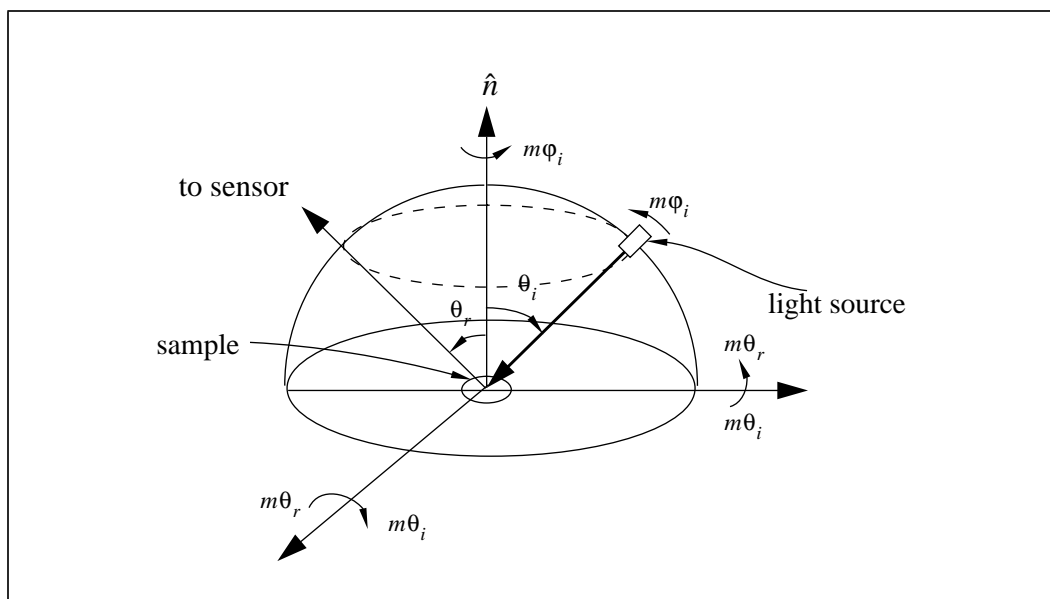


Figure 2.11 Free variables in the gonioreflectometer at Cornell

always measured with respect to the direction of illumination. In other words, there is no way to change ϕ_i and ϕ_r independently during a data scan. Note that the light detector is an array of spectra-radiometer, therefore it measures the BRDF as $f(\lambda)$.

There are other laboratories involved in BRDF measurement, such as NIST (National Institute of Standards and Technology). The NIST designed and built two instruments, the GOSI and the STARR, for diffuse and specular reflectance respectively [Germer97]. But we described here only the ones in computer graphics labs, as they are more comparable to our work.

2.5 Comments on Previous Works

Among the methods we described in the chapter, Murray's reflectometer and Cornell's gonioreflectometer used a light sensor as the light measuring instrument; Ward's reflectometer and the system used at Columbia University used a camera. The advantage of using a sensor is that its output range is usually larger than a camera. However, it also requires the incoming light to be evenly distributed over the sensor's viewing area. The advantage of using a camera is twofold. First, each pixel in the image is actually a tiny sensor, so it does not require the

incoming light to be evenly distributed over the camera lens' viewing area. Second, a 3-channel CCD camera gives response in RGB rather than one signal output of a sensor. Although different filters can be applied before the sensor to measure the reflectance in different wavelength band, it takes more time. Obviously, multi-channel CCD camera can be more efficient in measurement. The disadvantage of using a camera is its pixel output range is usually quite narrow. For an 8-bit camera, the pixel values are in the 0-255 range per channel.

Because BRDF requires huge amount of data, all the previous systems attempted to automate the process. However, none of them is totally automatic and human intervention is needed at some stage or even in the entire process. It is desirable to make the data acquisition as automatic as possible. It would be even more useful if the data acquisition can be remotely operated, so people can obtain the data from anywhere in the world. The goal of the work described in this thesis is to develop a system to measure the BRDF automatically after the initial setup, and allow users to do so over the Internet with their own program of measurement.

Chapter 3

System Description

The ACME measurement system used in this thesis is composed of computer controlled hardware, a light source, a CCD camera, and the computer software that controls them.

3.1 Equipment Description

Our BRDF measurement system includes a light source, a 3-channel CCD camera, a test station, a gantry on which the camera is mounted and a radiometer. Detailed description of each component is given in this section.

3.1.1 CCD Camera

The 3-channel CCD camera used in ACME is a Sony DXC-950. The various units of the camera are:

- A Sony 3-channel CCD color video camera DXC-950 head, which contains a three-chip Power HAD (Hole-Accumulated Diode) and an Automatic Gain Control device.
- A Sony Camera Adapter CMA-D2, whose input is the camera's output, and output is a monitor's input.
- A Sony RM-C950 Remote Control Unit.
- A Sony VCL-714BXEA Zoom Lens.

The Remote Control Unit can control camera's zoom, focus, f-stop, shutter speed and

white point adjustment [Sony950]. This is very important because through this unit these parameter can be adjusted by the computer.

3.1.2 Gantry

The gantry is actually a robot arm with five degrees of freedom. It includes a frame with three degrees of translation freedom and a PanTilt head with two degrees of rotation freedom. Thus the camera mounted on the gantry has five degrees of freedom. It enables the camera to be in any position within the gantry range and to point in any direction. The translational ranges of the gantry for x , y , z are 0-180cm, 0-178cm and 0-130cm respectively. The rotational ranges are 0-365° for azimuth and 0-95° for elevation.

3.1.3 Test Station

The test station is a platform with three degrees of freedom on which a test sample is placed. It consists of two translational motion stages mounted at right angles and a rotation stage mounted on top. The translational ranges are 0-31cm for x and 0-46cm for y . The rotational range is -360° to +360°. All stage motors have a linear accuracy of ± 0.00025 inch, and a rotary accuracy of 10 arc-min [Pai99].

3.1.4 Light Source

A diagram of the light source is shown in Figure 3.1. The light source is an incandescent lamp with a set of lenses. It gives an approximately parallel beam of 4cm in diameter. Filters can be added in front of the lens to produce beams of different ranges of wavelength. An aperture size can be adjusted to brighten or dim the beam. All the adjustments of the light source are manual.

3.1.5 Radiometer

The radiometer used in this experiment is an IL 1700 research radiometer/photometer made by International Light Inc. The dynamic output range is 1.0×10^{-19} Watt/cm² to $1.0 \times 10^{+19}$ Watt/cm². The detector is a silicon detector, model SED033, with 33 mm² receiving

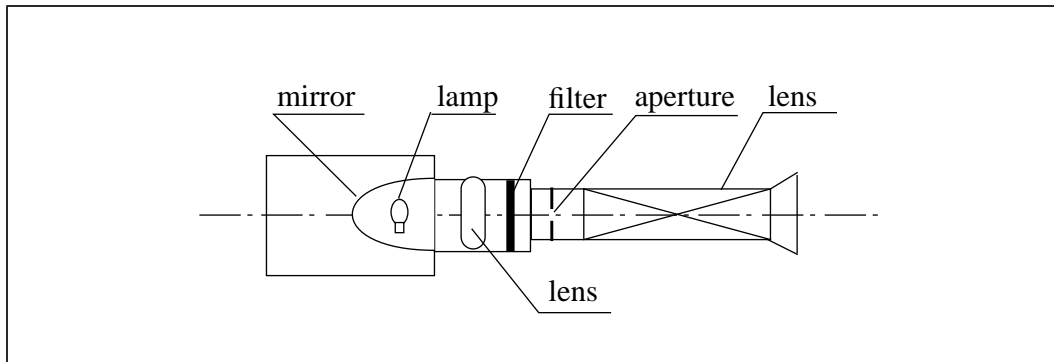


Figure 3.1 Light Source Structure

area. It gives a highly linear response to wavelength from 200 nm to 1100 nm, which covers the wavelength range of most visible light sources. For more information, refer to [IL1700] and web site <http://www.Intl-Light.com/products/il1700.html>.

3.1.6 Equipment Integration

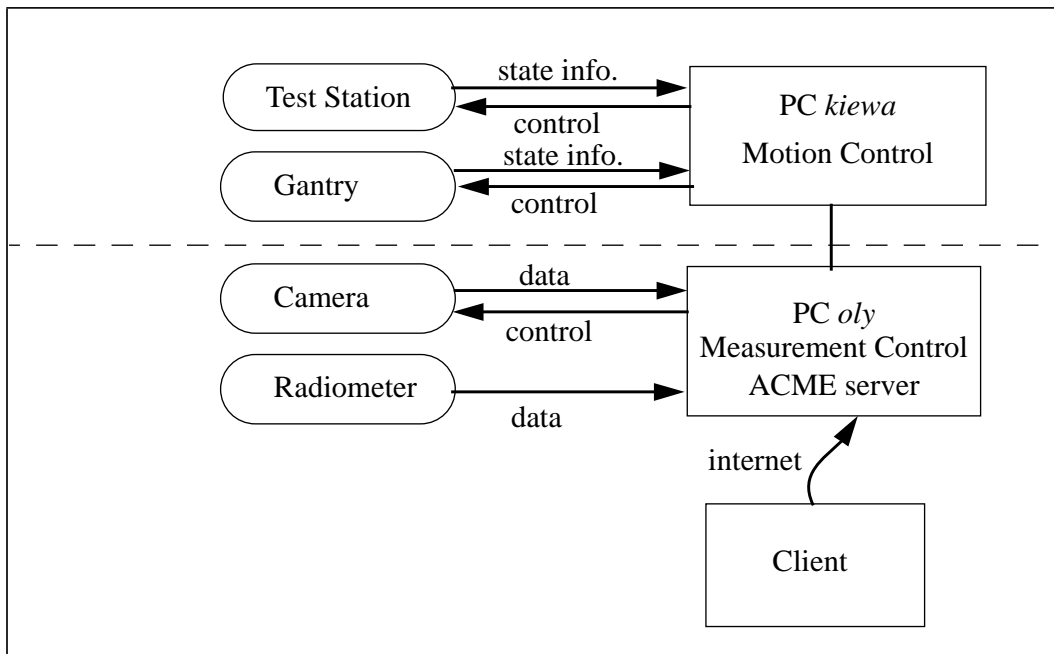


Figure 3.2 System connection Diagram

Figure 3.2 shows the integration of the equipment. The equipment can be divided into two groups, one is related to motion, the other is relevant to measurement. All of the motion equipment is connected to and controlled by a PC named *kiewa* which runs SunOS5.6. All the

measurement equipment is connected to and controlled by another PC named *oly* which runs *Linux* and is also called the *ACME server*. The reason why a separate PC is used to take care of motion is that motion control is a real time control and its completion time has to be guaranteed. Clients or experiment program can run on any other machine with proper authorization, as long as an internet connection to ACME server can be established. Figure 3.3 shows a picture of the ACME system in the configuration we used to measure a BRDF.

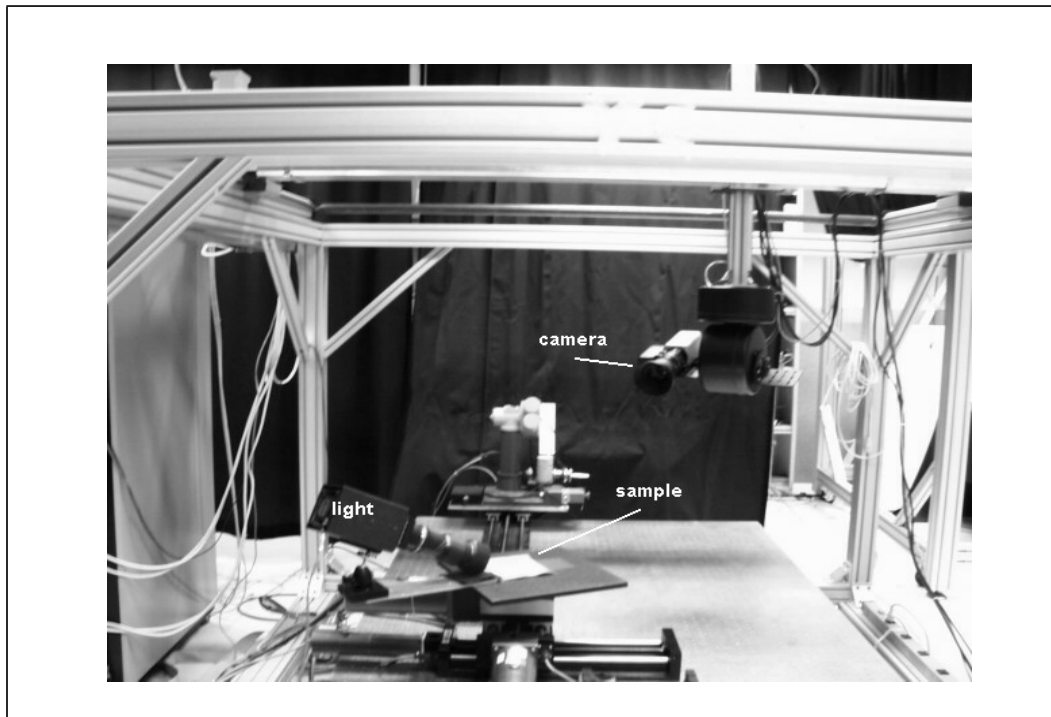


Figure 3.3 ACME system

3.2 Software Structure

ACME is designed for automatic remote measurements. Any machine which has web access and authorization can get connected to the ACME server and run an experiment. In order to enable different users on different operating systems to do experiments on ACME, Java has been selected as the primary programming language. Because of Java's platform independent nature, programs for experiment can be written anywhere in Java and will be uploaded from the client and executed on the ACME server. This relationship is shown in Figure 3.4.

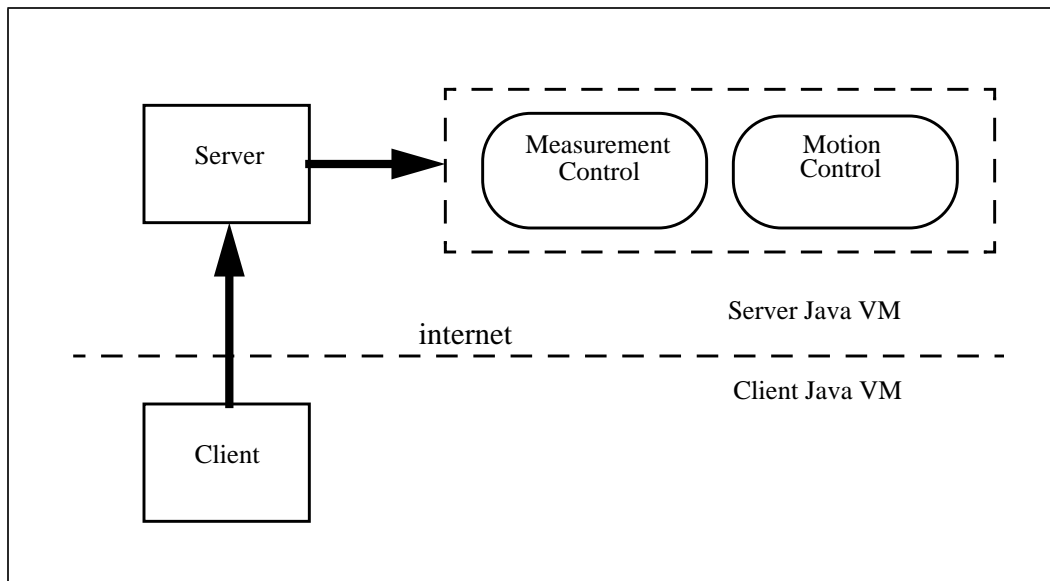


Figure 3.4 ACME software design

The Java classes of ACME are divided into several packages. The structure of ACME packages is illustrated in Figure 3.5. The basic interfaces are defined under the root package *acme*. There are five sub-packages under *acme* package: *acme.kinematics* which contains all the motion device controllers, *acme.server* which contains all the measurement device controllers, *acme.simulator* which contains the simulation of motion devices, *acme.viewer* which is in charge of the scene description and the viewing parameters, and *acme.utility* which contains some useful tools for programming.

In the *acme.kinematics* package, “*linear*” is a motion device with one degree of translation freedom, and “*puma*” is a robot arm with six degrees of freedom. In the *acme.server* package, “*rcclserver*” is a real-time robotic control server running on *kiewa* (the machine for motion control), and “*toflaser*” is a device which uses a time of flight laser to acquire 3D shape of objects. More details about the programming in ACME and user’s guide can be found at [/lci/project/acme/user/doc](#).

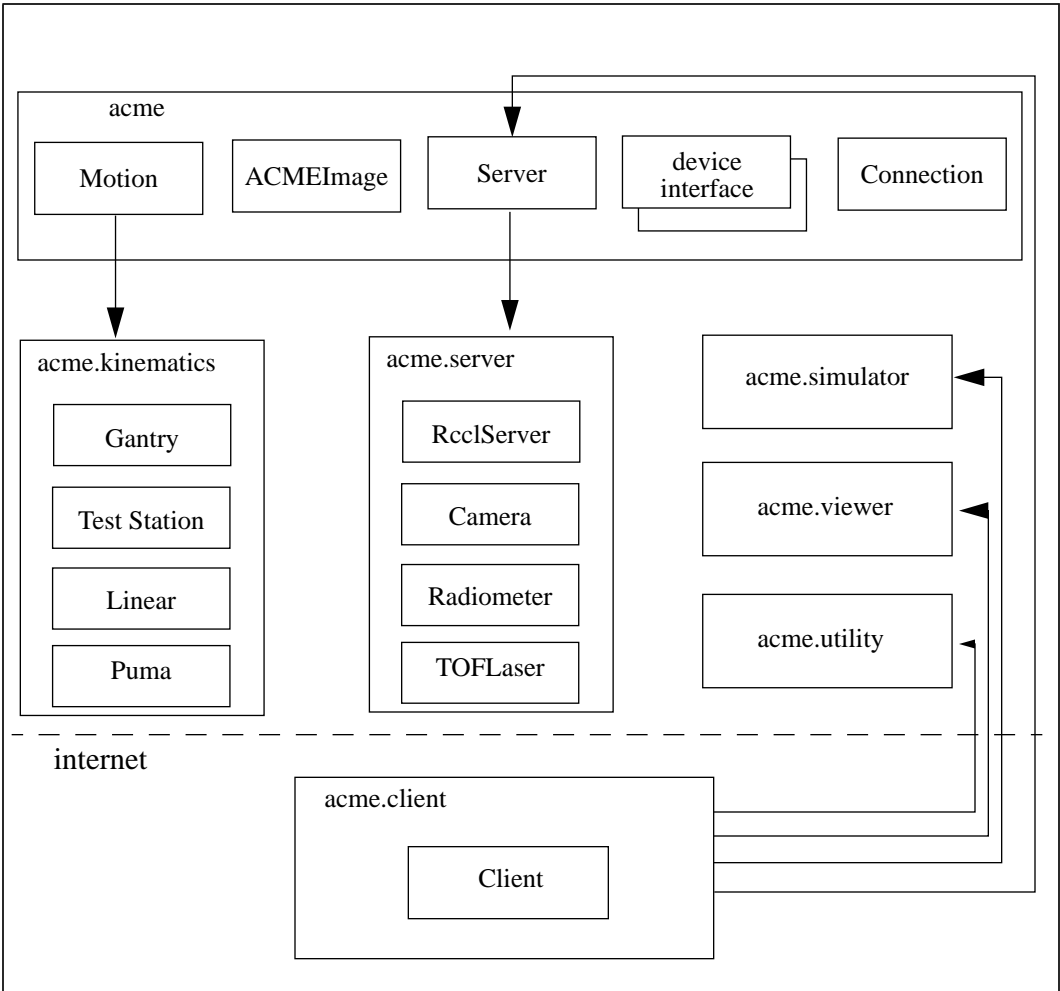


Figure 3.5 The structure of ACME packages

Chapter 4

Camera Calibration

4.1 Basic Principles of CCD Camera

The purpose of calibration is twofold. One goal is to convert the 3-channel image pixel value obtained from the camera to quantitative spectral value so that the experiment result can be compared to other standard data [PCG-98-1]. The other goal is to convert pixel values measured with different camera parameters into a “standard” value corresponds to a standard setting of camera parameters, so that pictures taken with different camera parameters can be compared to each other. The CCD camera’s output is a function of incident illumination strength, camera shutter speed and lens aperture opening.

CCD stands for *charge-coupled device* [PCG-96-1]. A CCD camera has three components: a CCD imager, amplification circuitry and a lens system [PCG-98-1]. The CCD imager is a particular type of silicon array imaging device containing an array (linear or two-dimensional array) of sensor elements. Light falling on the sensor elements (pixels) creates a charge (electron-hole pairs) due to the photoelectric effect. This charge is collected at each pixel by the formation of a potential well. The amount of charge collected at each pixel is linearly dependent on the light level, the exposure time and the camera aperture area until the potential well capacity is exceeded. For output, the collected charge is converted to voltage by an amplifier circuit, and gives rise to a signal. Thus the signal read from a CCD is proportional to the accumulated charge in the potential well of the sensor. The charge is proportional to the number of photons incident on the sensor area, and the number of photons represents the incident light strength. In principle, each CCD pixel can be used as a radiometer, i.e., we can use

this signal to derive quantitative information about the incident light.

Most CCD imagers have a silicon substrate. Silicon is opaque to light with wavelengths shorter than 400nm and transparent to light beyond 1100nm. Thus a CCD imager is useful only in the range between 400nm and 1100nm, which is more than enough to cover visible light. Within this range, different wavelengths have different capacities of creating charge by incident photons. This capacity is measured in terms of quantum efficiency (Figure 4.1) which indicates what percentage of photons of a particular wavelength hitting the front face of the CCD is converted into an electric charge. The quantum efficiency is always less than one and varies with the wavelength of light and the construction of the CCD.

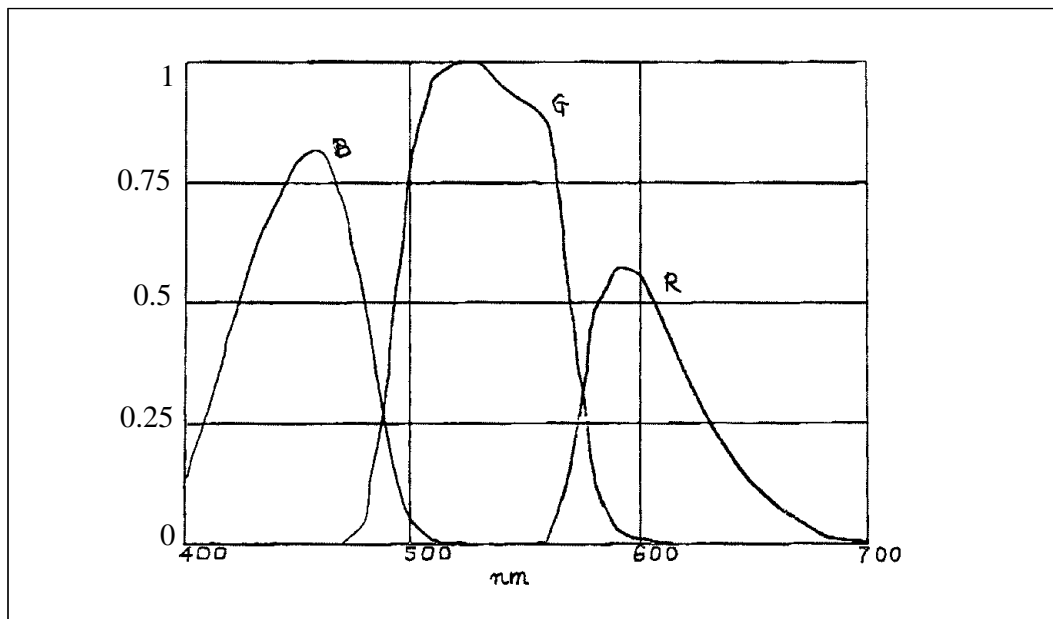


Figure 4.1 Spectral quantum efficiency curve of Sony DCX950 CCD camera (supplied by manufacturer)

4.2 CCD Camera Calibration

In principle, as mentioned above, the CCD camera's pixel values are proportional to the intensity of incident light with various factors. The validity of this principle must be verified before carrying out any quantitative measurements. In other words, calibration of the CCD camera against each variable parameter should be performed, while keeping all other

parameters fixed.

4.2.1 Calibration for Source Radiance

Source radiance $L(\lambda)$ is a function of wavelength. Common light sources cover a range of wavelengths. For a specific light source, its wavelength distribution is fixed. In the following calibration, the light source used was the one described in section 3.1.4. By varying the intensity of the light source and measure it with both a radiometer (see section 3.1.5) and the camera (see section 3.1.1), we get a relationship between the radiometer reading and the average pixel value over the three channels of the camera. If we treat the radiometer reading as the “true” light intensity, then camera pixel value can be calibrated. Figure 4.2 shows a plot of camera pixel value vs. radiometer reading, with the camera setting of f-number = 120 and shutter-speed = 100. This setting will be used as the “standard pixel setting”.

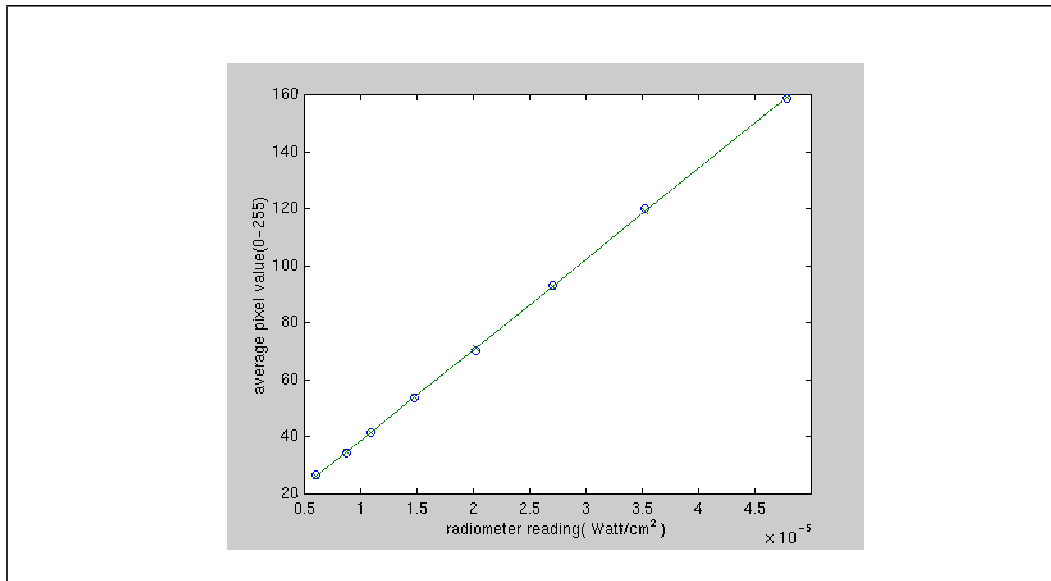


Figure 4.2 Pixel value as a function of radiometer reading

The curve in Figure 4.2 is a linear fit in a least-square sense. The function is

$$p = (3.19 \times 10^6) E + 6.80 \quad (\text{Eqn 4-1})$$

where p is pixel value and E is radiometer reading in W/cm^2 . The standard deviation of this linear fit is 0.64. If the average pixel value throughout the measurement lies halfway between

0 and 255, the error incurred by this linear fit is only about 0.5%. The inverse function of (Eqn 4-1) is,

$$E = (3.13p - 21.3) \times 10^{-5} \quad (\text{Eqn 4-2})$$

This inverse function can be used to convert camera pixel value (0-255) to irradiance (see Appendix A). Theoretically, a pixel value is not directly related to irradiance, but to radiance. The relationship between these two in a camera is (see Figure 4.3):

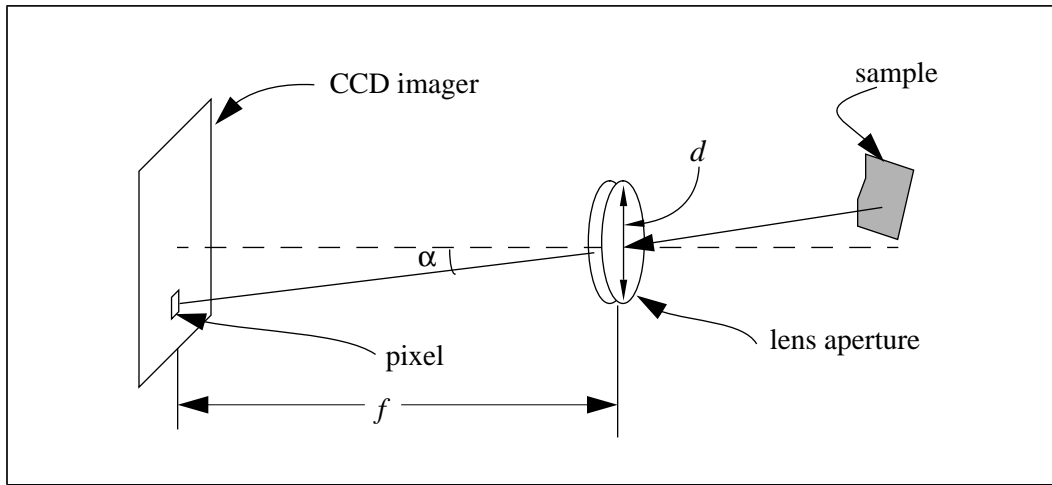


Figure 4.3 Image forming system

$$E = \frac{\pi}{4} \left(\frac{d}{f} \right)^2 \cos^4 \alpha \cdot L \quad (\text{Eqn 4-3})$$

where d is the diameter of camera lens' aperture, f is the focal length and α is the angle between the pixel and the optical axis of the camera ($\alpha = 0$ at the center of the image) [Horn79]. This shows that the radiance and irradiance are proportional for a given pixel. We will use here the irradiance for the standard setting as determined by (Eqn 4-2) (see also section 5.3.2 and 5.3.3).

4.2.2 Calibration for Exposure Time

Assuming that the intensity of the light beam does not change over time and the CCD elements are not saturated, pixel value and exposure time should be linearly related. Hence the

plot of pixel value vs. exposure time should be a straight line. Figure 4.4 shows this relation as measured. The linear function is:

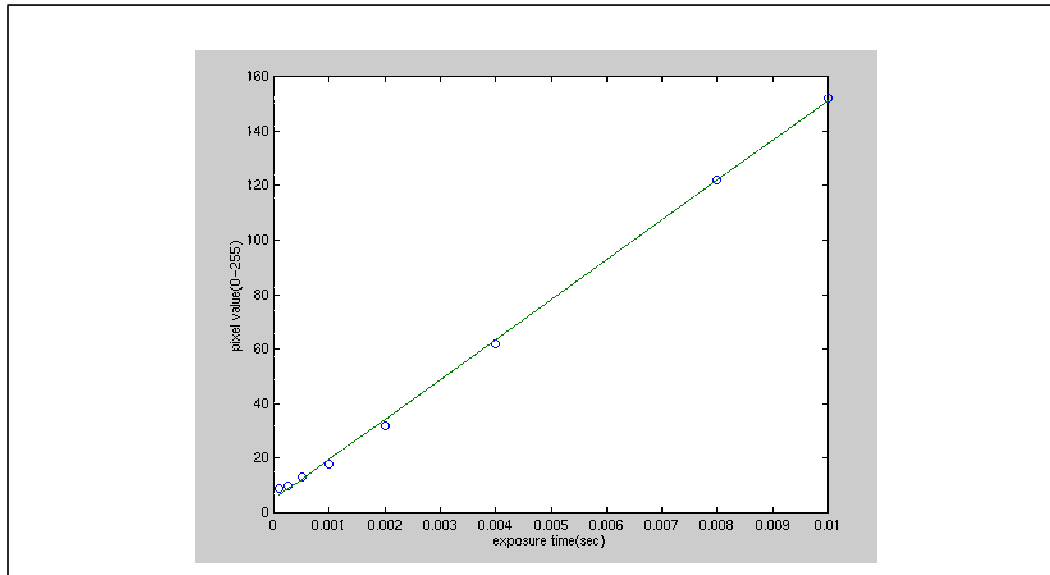


Figure 4.4 Pixel value as a function of exposure time

$$p = (1.46 \times 10^4)t + 5.10 \quad (\text{Eqn 4-4})$$

where p is pixel value and t is exposure time in second. The standard deviation of this linear fit is 1.55. If the average pixel value throughout the measurement lies halfway between 0 and 255, the error incurred by this linear fit is about 1.5%.

4.2.3 Calibration for F-number

F-stop, or aperture values, are related to the size of the opening that light passes through in the rear of lens. Usually f-stop is calculated by the ratio of the focal distance of the lens over the aperture diameter. The smaller the f-stop, the more light gets through the lens, and the brighter the images will be. For the CCD camera we used, the f-stop can be set as a f-number which ranges from 0 to 255. The relation between the f-number and commonly used f-stop numbers is not stated. The calibration gives a square relationship, which means the f-stop of the camera is proportional to the inverse square of the f-number. Given the square relationship between the aperture's diameter and the aperture's area, the pixel value should be propor-

tional to the 4-th power of the camera f-number. Figure 4.5 shows the relation of pixel value vs. the 4-th power of f-number.

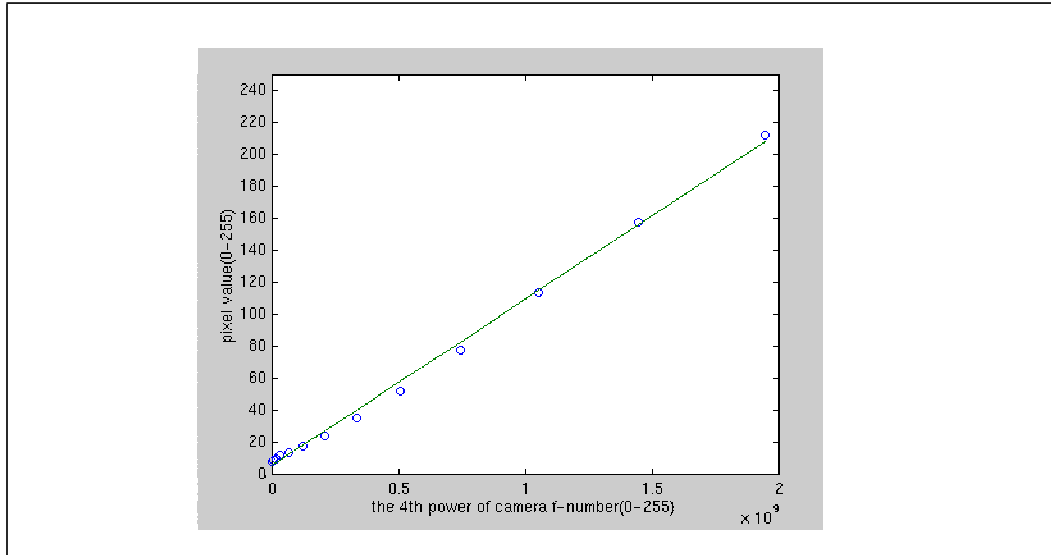


Figure 4.5 Pixel value as a function of the 4-th power of camera f-number

From Figure 4.5, we can see that the relation is approximately linear. The result agrees with our analysis in section 4.1. And the function is

$$p = (1.04 \times 10^{-7}) fn^4 + 5.87 \quad (\text{Eqn 4-5})$$

where p is pixel value and fn is camera f-number. The standard deviation is 3.32. If the average pixel value throughout the measurement lies halfway between 0 and 255, the error incurred by this linear fit is about 3%.

4.3 Standard Pixel Value and Irradiance

As a result of the calibration, given a pixel value p , with a shutter speed s , which is the inverse of exposure time t , and a f-number fn , the standard pixel value can be calculated by:

$$p_s = \frac{120^4}{fn^4} \cdot \frac{s}{100} \cdot (p - 5.87) + \frac{0.77 \cdot s}{100} + 5.1 \quad (\text{Eqn 4-6})$$

and the irradiance E can be calculated by:

$$E = \left(3.13 \cdot \frac{120^4}{fn^4} \cdot \frac{s}{100} (p - 5.87) + 3.13 \cdot \frac{0.77 \cdot s}{100} - 5.3 \right) \times 10^{-5} \quad (\text{Eqn 4-7})$$

See section 5.3.2 for the derivations of these equations.

Chapter 5

Data Acquisition and Treatment

5.1 Size of Test Sample

Since we do not want to capture the texture, which is the variation of reflectance on the surface, the smaller the sample size the more accurate the experiment result will be. However too small a sample covers too few pixels in the CCD image, especially when the angle from which the camera sees the sample is close to 90° from the normal of the sample surface. This will increase the difficulty in the images processing on locating the sample pixels.

In our experiments, the sample size is 15mm in diameter, which is big enough for post image processing and small enough to be evenly illuminated by the light source. Also, the sample is a round patch which creates the same elliptical shape under the same elevation angles. This simplifies the image processing of experimental data.

If the experiment involved the use of a radiometer, however, sample size would have to be reconsidered. A radiometer uses a barrel to prevent side light coming to the sensor. Therefore, the sample size should be calculated from the barrel's viewing angle, the distance between the sensor and the sample, and the angle from which the sensor sees the sample. For details, refer to Appendix A.

5.2 Data Acquisition Steps

Since BRDF measurement requires four degrees of freedom, and ACME provides fif-

teen degrees of freedom altogether, there are more than one way to design the experiment.

First, we can place the sample on the center of the test station and attach the light source on the test station as well (see Figure 5.1). Thus the motion of the test station will not cause any change in relative position between the sample and the light source. With the gantry's position fixed and rotating the test station, the camera can "see" the sample from different azimuth angles; and by moving the gantry, we can create different elevation angles. The advantage of this method is that for a fixed elevation view angle, it only involves one motor (for rotation) in the experiment. This makes it easier for collision detection, and involves less error due to the motion devices. The disadvantage is that the light source has to be attached to the test station. This limits the distance between the light source and the sample, and makes it difficult to give an incident angle θ_i close to 90° .

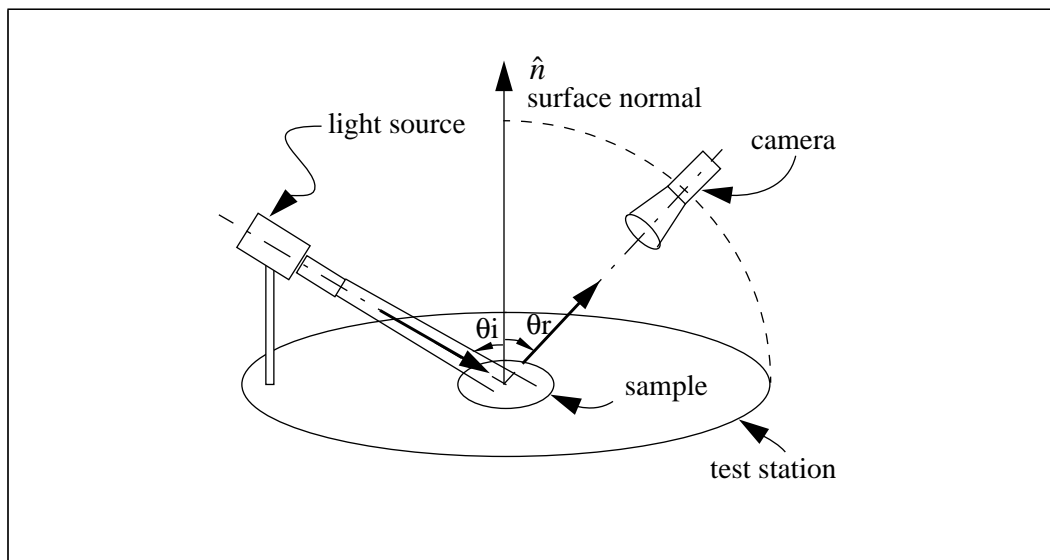


Figure 5.1 Devices when sample and light are attached to test station

Another method is to place the sample on the test station's platform, fix the light source on the test bed, and move the gantry around the sample to take pictures. Since the gantry has five degrees of freedom, it is enough for changing the reflected direction in the BRDF measurement. The advantage of this method is that it is easy to set up the experiment, and the light source can be placed anywhere as long as it illuminates the sample. The disadvantage is

that for each image taken at least four motors are involved. This requires a better collision detection algorithm, introduces more errors due to motion and takes longer time.

In our experiment, the first method is employed. While taking images, the camera's f-stop and shutter speed are adjusted to make the pixel values within 20-250. Concrete steps are:

Step 1. Position the light source on the test station platform. Adjust the height of the light source to change the incident elevation angle.

Step 2. Move the camera to a position exactly above the sample center. In other words, move the camera's axis onto surface normal \hat{n} in Figure 5.1. This can be achieved by moving the gantry in x-y plane or move the test station, until the sample centers at the center of image grabbed by the camera.

Step 3. Adjust the camera's f-stop and shutter speed until the sample pixel's RGB values are in the range between 20 to 250. This is because the RGB value ranges from 0 to 255 for a 3-channel 8-bit camera. If the signal is too weak compared to the background, it is hard to recognize in post image processing and the signal to noise ratio is high. If the signal is close to 255, it is close to overflow. And the camera response tends to be non-linear when pixel value is near to overflow.

Step 4. Take an image. If azimuth < 360 degree, rotate the test station to next azimuth angle and go to step 3. Otherwise go to step 5.

Step 5. Move the gantry to next elevation position, and go to step 3.

5.3 Image Post Processing

If the elevation interval is 10 degrees and the azimuth interval is 20 degrees, $9 \times 18 = 162$ images are obtained for one incident direction. An example image is given in Figure 5.2. For each of these images with different camera f-stop and shutter speed, the pixel value in the center of the sample area is extracted, and converted to a "standard" pixel value or

to irradiance according to different needs (see section 5.3.2 and 5.3.3).



Figure 5.2 An image captured by CCD camera

5.3.1 Locating the Sample in the Image

Given the condition that the background is dark enough compared to the sample area, the sample area can be found by locating pixels whose RGB value is bigger than a threshold. Since the camera is approximately pointing to the center of the sample, the sample area should be roughly at the center of an image. By examining the central area of an image, a bright spot can be found. Threshold is dynamically adjusted to adapt each image. The concrete steps to locate the sample in an image are:

Step 1. Set $\text{threshold} = 100$, $\text{increase_flag} = 0$, $\text{decrease_flag} = 0$.

Step 2. For each pixel in the central area of the image, if its value is bigger than the threshold, treat it as a “seed” of a bright spot. Check all neighbouring pixels of a seed. If their values are also bigger than the threshold and not in the bright spot pixel group, add them to it and make them to be new seeds. Repeat this process until no neighbouring pixel can be added. If the number of pixels is too small, i.e., less

than 60, discard that spot.

Step 3. If exactly one bright spot is found, treat this as the sample spot and go to step 6.

Otherwise, go to step 4.

Step 4. If no spot was found and `increase_flag == 0`, lower the threshold by 20, set `decrease_flag = 1` and go to step 2. Otherwise go to step 5.

Step 5. If more than one bright spots are found and `decrease_flag == 0`, increase threshold by 20, set `increase_flag = 1` and go to step 2. Otherwise give a warning that threshold can not be adjusted to admit only one bright spot in the image, take the bright spot with largest number of pixel as the sample area and go to step 6.

Step 6. Find the sample area's central position by finding the pixel that the number of pixels above it is closest to the number of pixels below it, and the number of pixels on its left is closest to the number of pixels on its right. Calculate the average pixel value of the center pixel and its 8 neighbours, then pass the value with camera's f-stop and shutter speed to convert pixel value to the standard value (Section 5.3.2).

The reason why we discard bright spots with very small number of pixels is that they cannot be the sample area. These small bright spots may be a screw on the platform or some other artifacts.

The purpose of using the `increase_flag` and `decrease_flag` is to prevent a tight loop. It is possible that when the threshold is 100, more than one bright spots can be found. But if the threshold decreased to 80, no spots can be found. If we do not have the increase and decrease flags, the system may increase and decrease the threshold back and forth.

The reason why we take the bright spots in the images as the sample area is that the current motion system can not guarantee that the center of the image, i.e. (320,240) in a 640x480 image, is the sample center. By taking the bright spot as sample area, we assume that

the sample area is brighter than other areas in the image. This is not always true, especially when measuring some material that absorbs most of the energy incident to it. If we can accurately adjust the camera's pointing direction to be exactly at the sample center, the image processing will be very simple — just take the value of the pixel at the image center as the sample pixel value.

5.3.2 Converting to Standard Pixel Value

Since the pixel values obtained so far are associated with different camera f-stops and shutter speeds, they have to be standardized in order to be compared to each other. In the conversion below, we take f-stop = 120, shutter-speed = 100 as the standard condition. Pixel values with other f-stop or shutter-speed are converted to a value corresponding to the standard condition. In other words, we enlarged the camera's output range by setting its parameters.

During the experiment, camera's f-number varied from 120 to 180. From Figure 4.5 and (Eqn 4-5), we know that the pixel values are proportional to the 4-th power of camera f-number. Suppose p is the pixel value before any conversion, the pixel value after f-number conversion is

$$p_f = \frac{120^4}{fn^4} \cdot (p - 5.87) + 5.87 \quad (\text{Eqn 5-1})$$

where p_f is the pixel value after f-number correction, and fn is the camera f-number.

As we know, camera's shutter-speed is defined as the inverse of the exposure time. We selected the shutter speed of 100, 125, 250, 500 and 1000 during the experiment. The available non-flicker shutter speeds of our camera are 100, 125, 250, 500, 1000, 2000, 4000 and 10000. The reason why we exclude those very high speed is that the opening and closing operation of camera's shutter need some time. Ideally this operation time should be zero. Practically, every particular camera has its specific operation time. Thus the higher the shutter speed is, the less exposure time is, the more significant the error introduced by camera operation time.

As we take the shutter speed = 100 to be the standard one, according to Figure 4.4 and (Eqn 4-4), the conversion from other shutter speed is,

$$p_s = \frac{s}{100} \cdot (p_f - 5.1) + 5.1 \quad (\text{Eqn 5-2})$$

where p_s is the standard pixel value, and s is the camera's shutter speed.

Substitute (Eqn 5-1) into (Eqn 5-2), the standard pixel value for an original pixel value of p is

$$p_s = \frac{120^4}{fn^4} \cdot \frac{s}{100} \cdot (p - 5.87) + \frac{0.77 \cdot s}{100} + 5.1 \quad (\text{Eqn 5-3})$$

This is true for each of the three channels of the camera. Since the sensitivity of human eye is different for different channels, luminance values need to be calculated from the R, G and B pixel values as:

$$Y = 0.30p_R + 0.59p_G + 0.11p_B \quad (\text{Eqn 5-4})$$

where Y represents human eye perceived brightness. Thus the pixel values are converted to photometric quantities related to luminance sensitivity.

5.3.3 Converting to Radiance Value

In most computer graphics systems, brightness quantities are simply denoted by a number, or RGB triplets in colour systems. These numbers are used to specify many quantities including light source, material properties and intermediate calculations. They have relative meanings to each other, but are not physical units. In order to compare our experiment data to data from other laboratories, BRDF measurement results should be converted to radiance value. According to the linear calibration in section 4.2.1, standard pixel value can be converted to irradiance by (Eqn 4-2). As we mentioned in section 4.2.1, the radiance and irradiance hold a linear relation to each other by (Eqn 4-3). Since the sample area in an image is approximately at the center, the angle between the pixel and the optical axis of the camera is very small ($\alpha < 0.2^\circ$ in our experiments). If we take $\alpha = 0$ (for the pixel at the center of an

image) in (Eqn 4-3) and combine (Eqn 4-2) and (Eqn 4-3) together, the standard pixel value p_s can be converted to radiance in $\text{W}/\text{cm}^2/\text{sr}$ by,

$$L = \frac{4}{\pi} \left(\frac{f}{d} \right)^2 \cdot (3.13p_s - 21.3) \times 10^{-5} \quad (\text{Eqn 5-5})$$

where d is the diameter of camera's aperture, f is the focal length (see Figure 4.3), and $\frac{f}{d}$ is the camera's f-stop (see section 4.2.3 for definition).

Chapter 6

Results and Analysis

Two sample materials were measured. The first sample is a piece of white 20-lb WEY-ERHAEUSER recycled husky Xerocopy paper. The second sample is a piece of red silk.

6.1 Isotropic Check

Before measuring its BRDF, we want to know whether a material is isotropic or anisotropic. For an isotropic material, its BRDFs is independent of $\varphi_i - \varphi_r$ (see Figure 1.1). Given this definition, isotropic characteristic of a material can be determined by observing the changes in the reflectance of a sample while rotating the sample and fixing both camera and light source positions¹. This actually keeps constant θ_i , θ_r , and $\varphi_i - \varphi_r$, and changes φ_i . If the reflectance does not vary in this process, the material is isotropic; otherwise, it is anisotropic.

For each material used, an isotropic check was done with $\theta_i = 65^\circ$ and 45° , $\theta_r = 50^\circ$ and 80° , and $\varphi_i - \varphi_r = 180^\circ$. Figure 6.1 to Figure 6.4 show the results of a piece of white photocopy paper (sample 1), and Figure 6.5 to Figure 6.8 show the results of a piece of red silk (sample 2). In all the figures of isotropic checks, the angles marked in every 30 degrees are φ_i , and the values are the average pixel values over the three channels RGB. We can see that the paper is not strictly isotropic, but within 10%, while the silk is far from isotropic,

1. In the general case, one can determine if a BRDF is isotropic from the whole BRDF (see [DeYong97]). But here we want to test this before measuring it, so our determination is necessarily incomplete.

especially when θ_r is close to 90° .

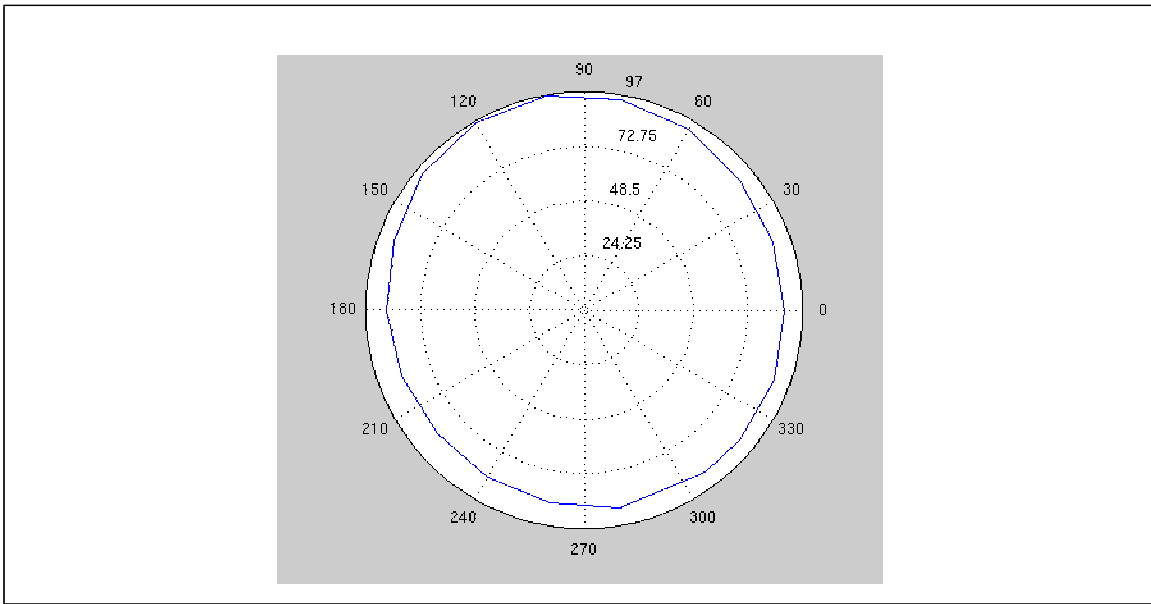


Figure 6.1 Isotropic check of white paper with incident angle of 65° and view angle of 50°

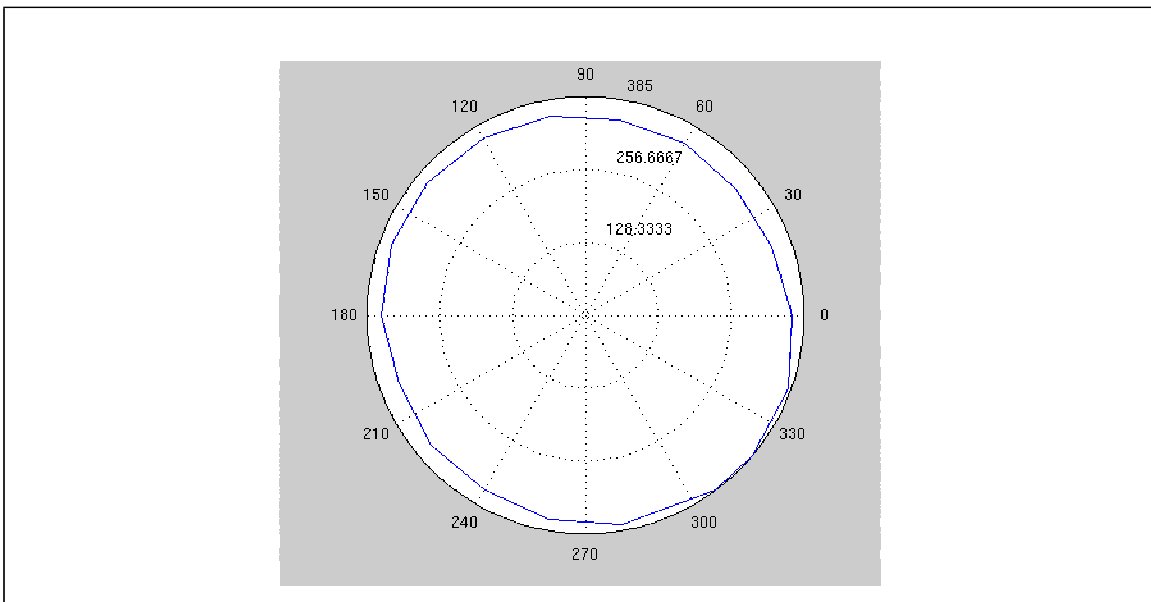


Figure 6.2 Isotropic check of white paper with incident angle of 65° and view angle of 80°

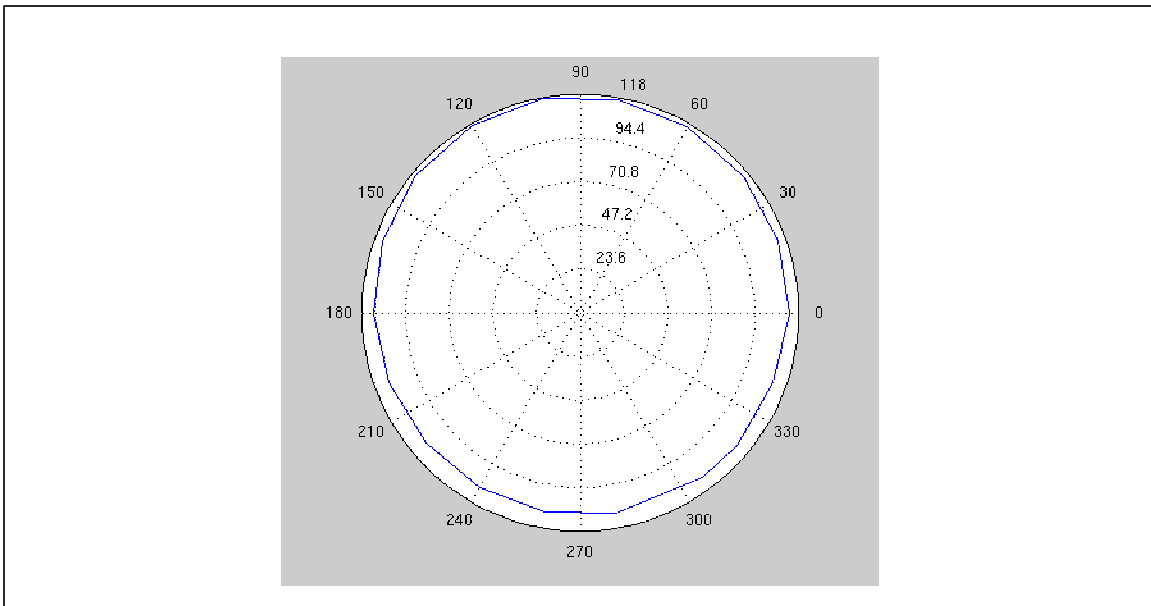


Figure 6.3 Isotropic check of white paper with incident angle of 45° and view angle of 50°

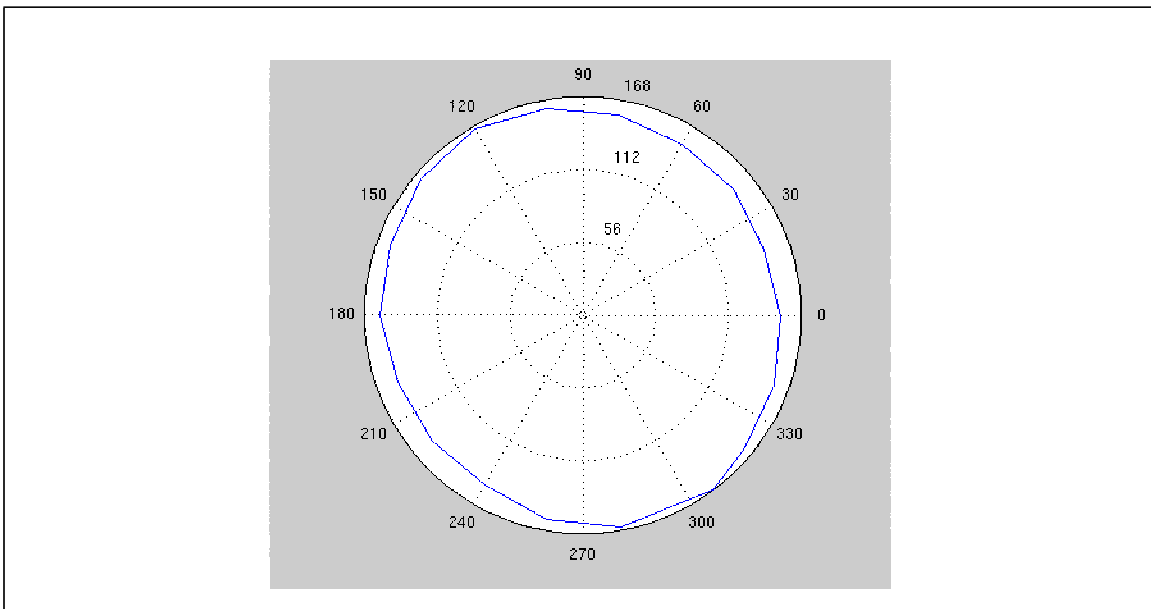


Figure 6.4 Isotropic check of white paper with incident angle of 45° and view angle of 80°

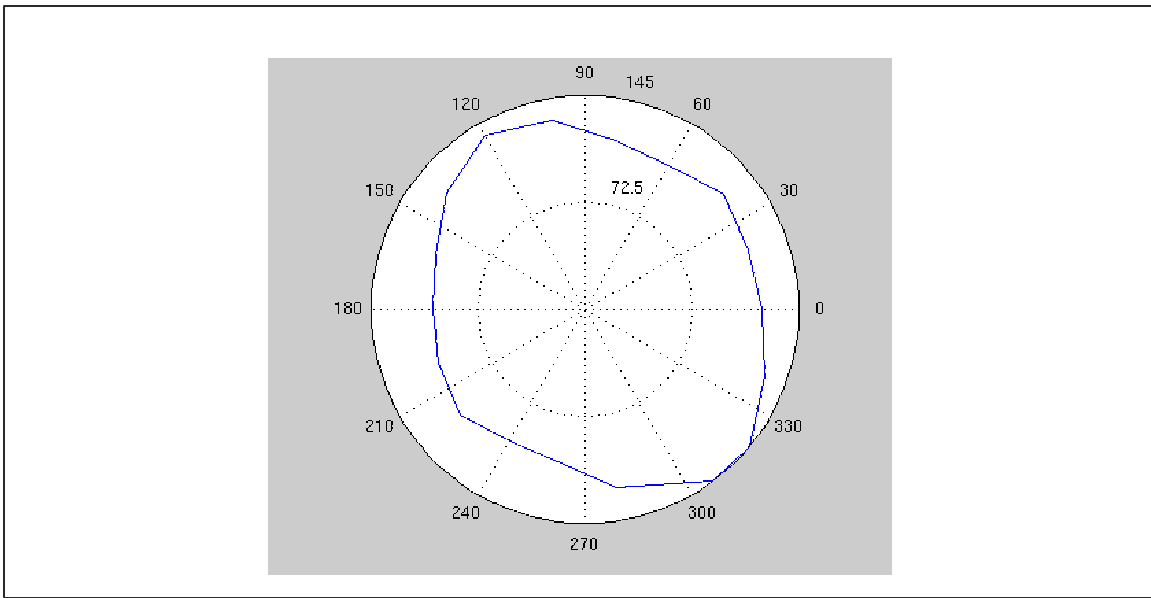


Figure 6.5 Isotropic check of red silk with incident angle of 65° and view angle of 50°

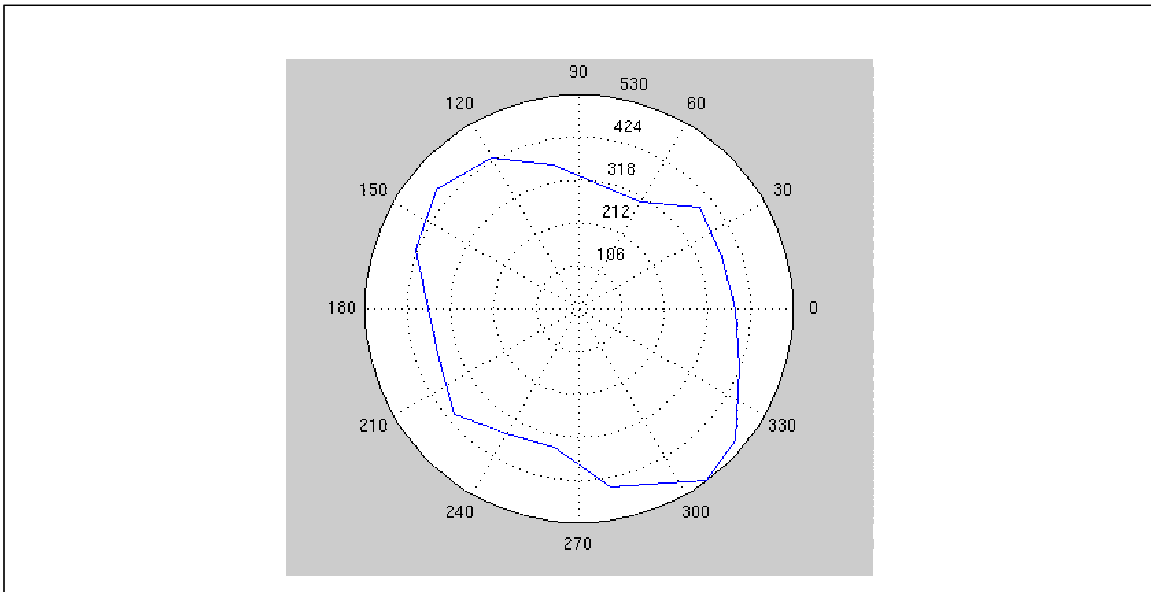


Figure 6.6 Isotropic check of red silk with incident angle of 65° and view angle of 80°

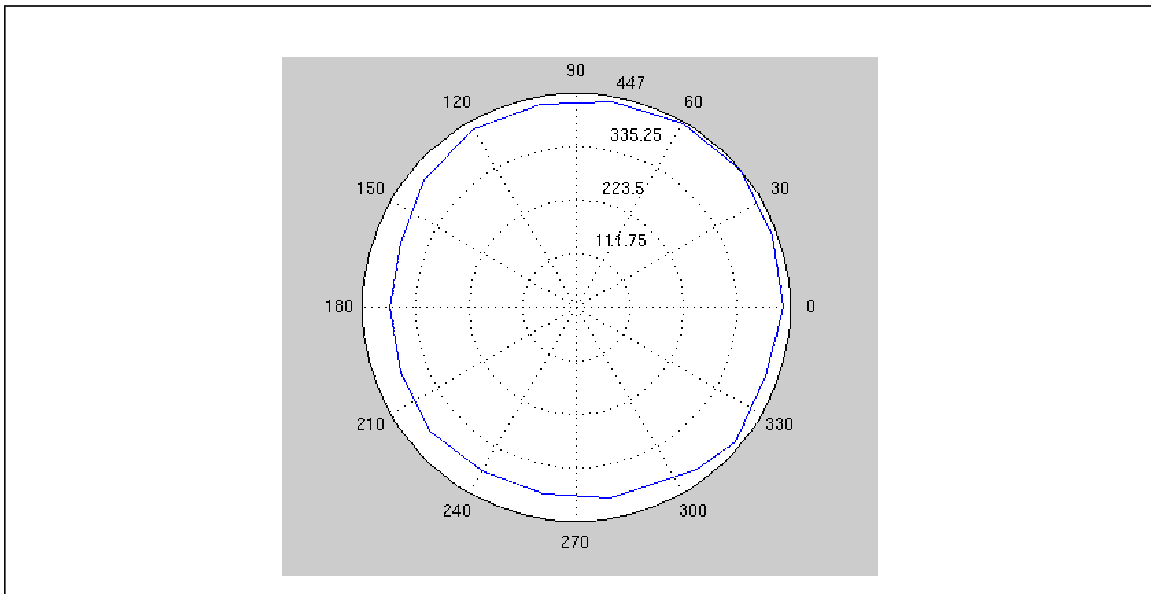


Figure 6.7 Isotropic check of red silk with incident angle of 45° and view angle of 50°

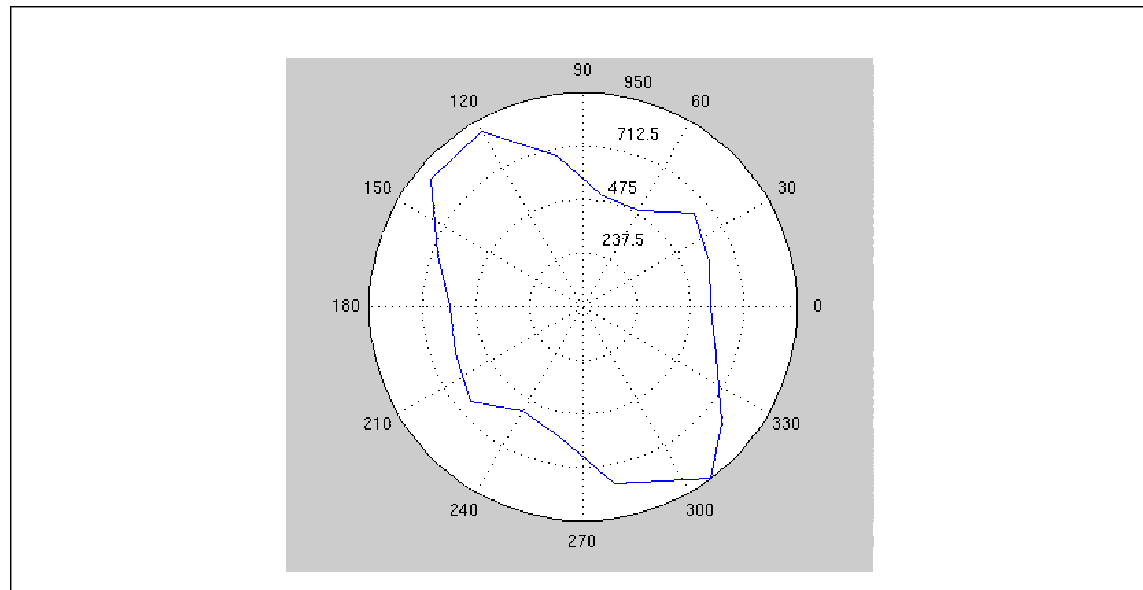


Figure 6.8 Isotropic check of red silk with incident angle of 45° and view angle of 80°

6.2 Bidirectional Reflectance

6.2.1 Sample 1: Plain Paper

From the isotropic check, we know that the paper is not strictly isotropic, but we will treat it as such material in the following experiments, which means that we ignored the influ-

ence of $\phi_i - \phi_r$. Figure 6.9 to Figure 6.11 show the BRDFs for an incident light of $\theta_i = 65^\circ$. Figure 6.12 to Figure 6.14 show the BRDFs of $\theta_i = 45^\circ$. The view points (azimuth, elevation) are at $(-45^\circ, 50^\circ)$ in the side view figures and $(0^\circ, 90^\circ)$ in the overhead view figures.

We can see that for smaller incident angles (e.g. $\theta_i = 45^\circ$, see Figure 6.12), the reflection around the opposite direction is stronger than other directions, and it is almost evenly distributed in directions further from the opposite direction. For larger incident angles (e.g. $\theta_i = 65^\circ$, see Figure 6.9), the reflection in directions close to the incident is similar to that of smaller incident angles (Figure 6.12), but much stronger in the opposite direction. This is a phenomenon that we can verify by looking at a piece of paper from a direction close to its surface tangent with a light on the opposite side. In this case the paper appears very bright. Another phenomenon is that the BRDFs of paper is almost symmetrical.

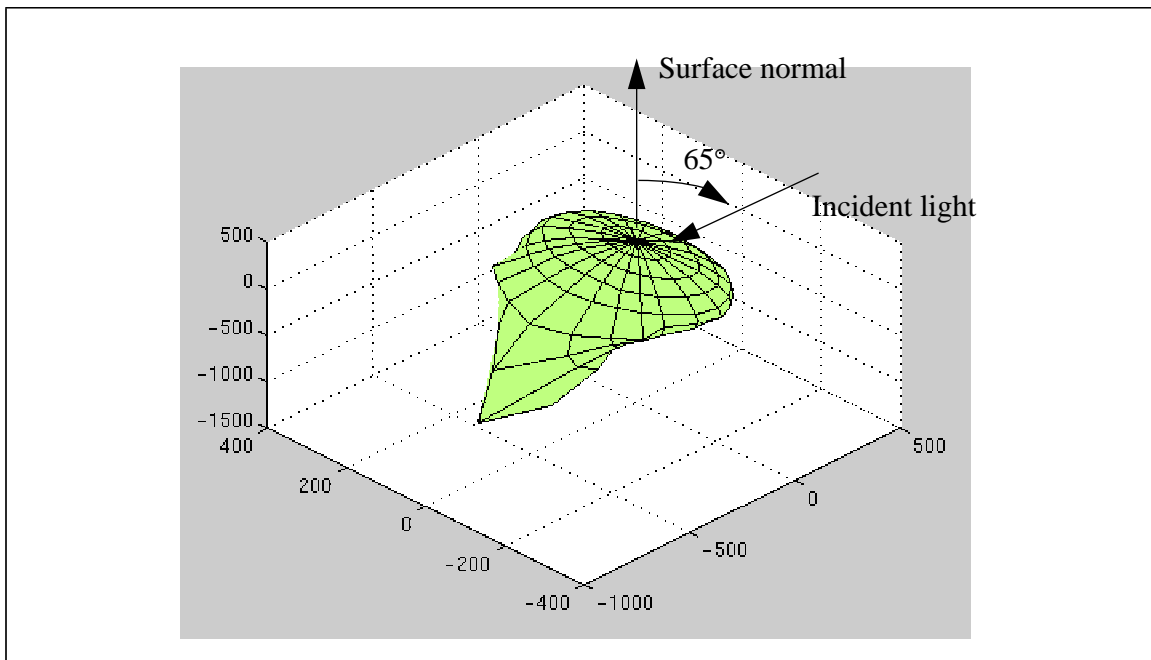


Figure 6.9 Side view of white paper's BRDFs with the incident direction at 65° to the right

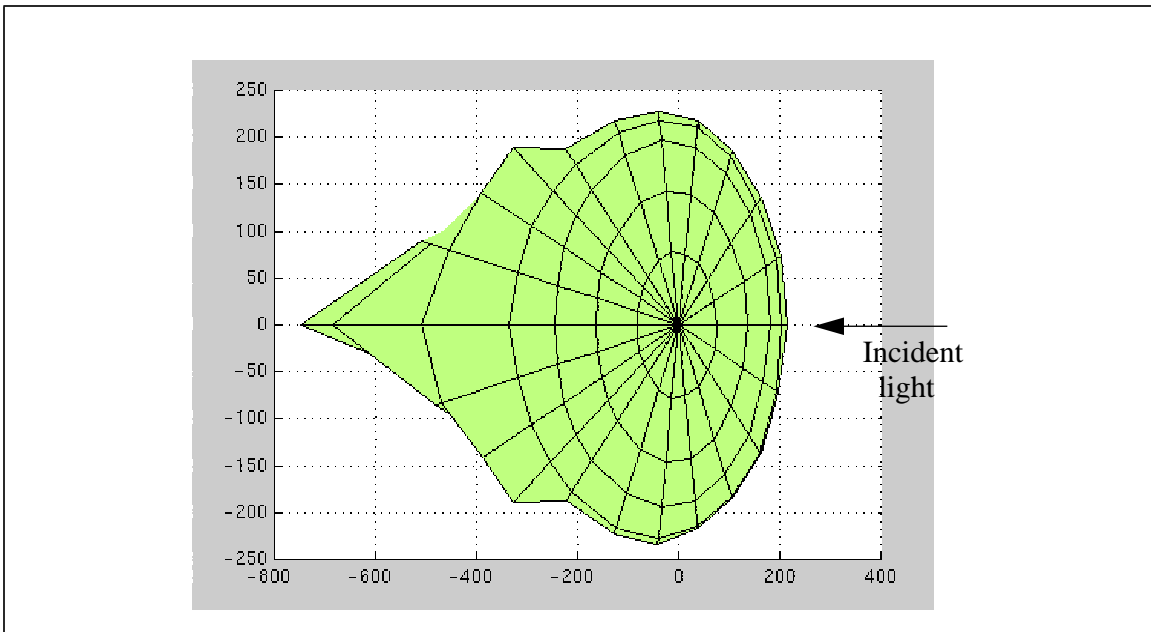


Figure 6.10 Overhead view of white paper's BRDFs with the incident direction at 65° to the right

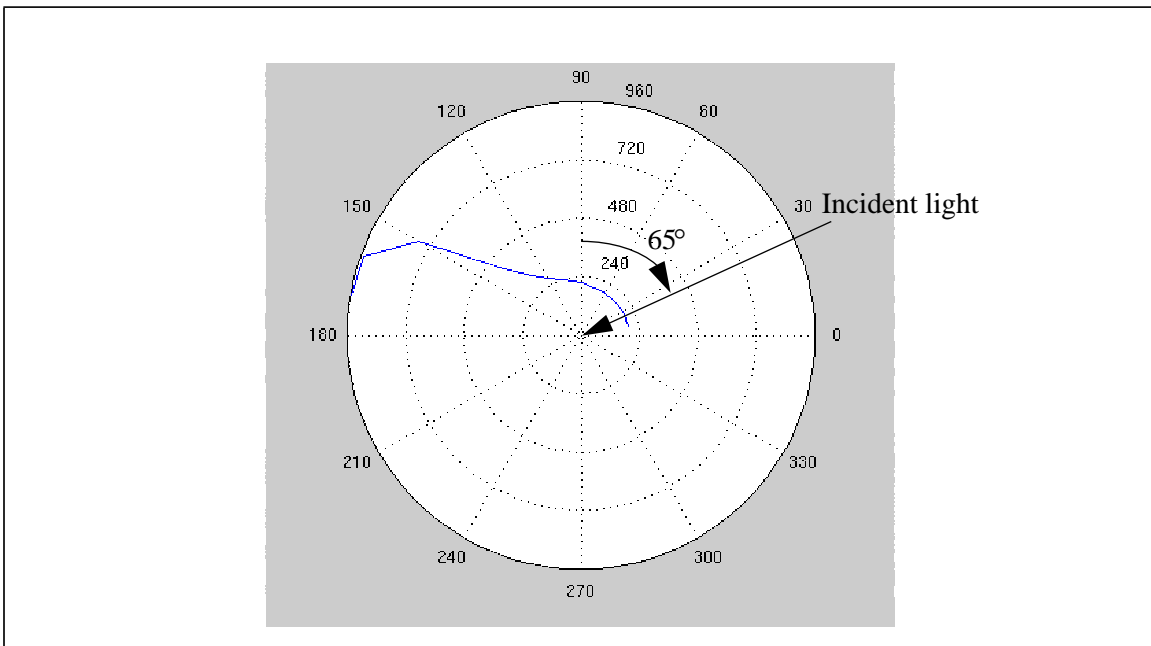


Figure 6.11 The incident plane of white paper's BRDFs with the incident direction at 65° to the right

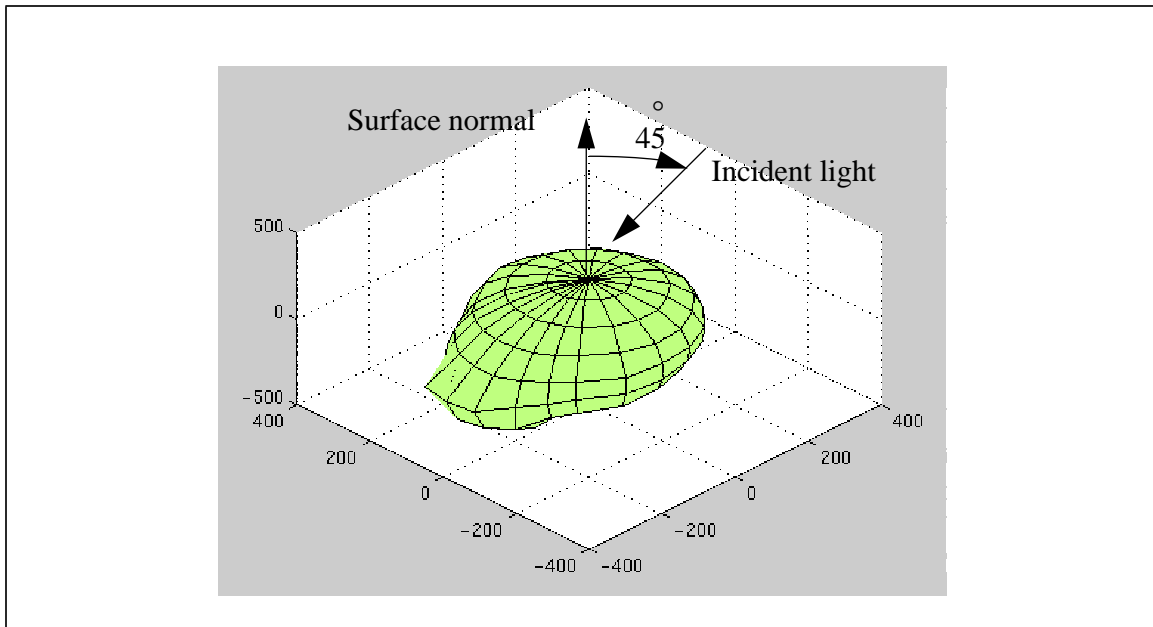


Figure 6.12 Side view of white paper's BRDFs with the incident direction at 45° to the right

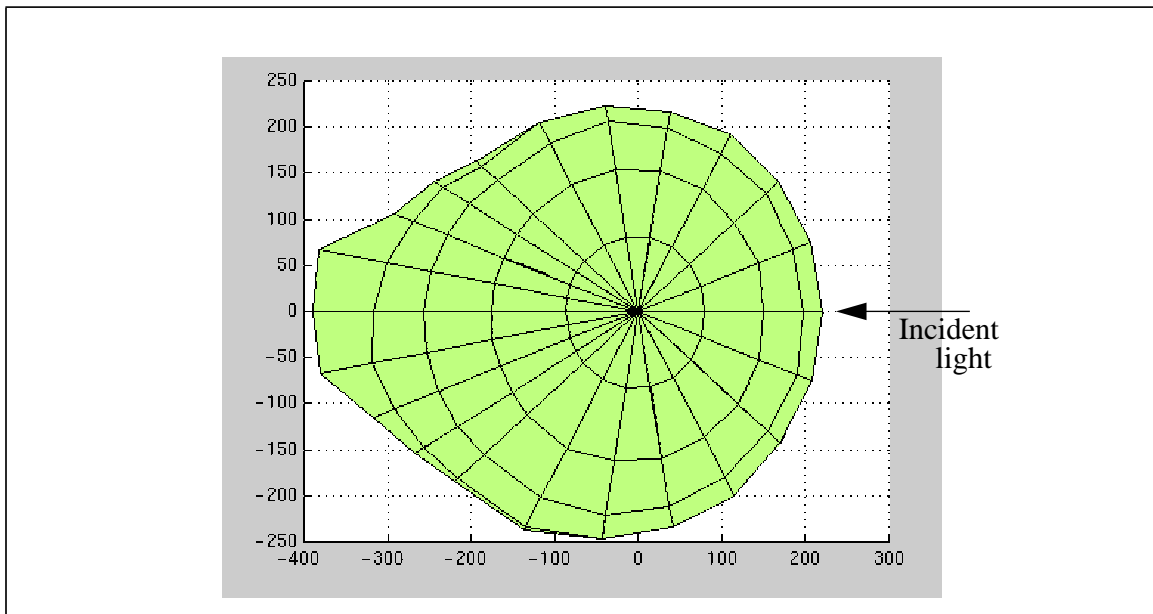


Figure 6.13 Overhead view of white paper's BRDFs with the incident direction at 45° to the right

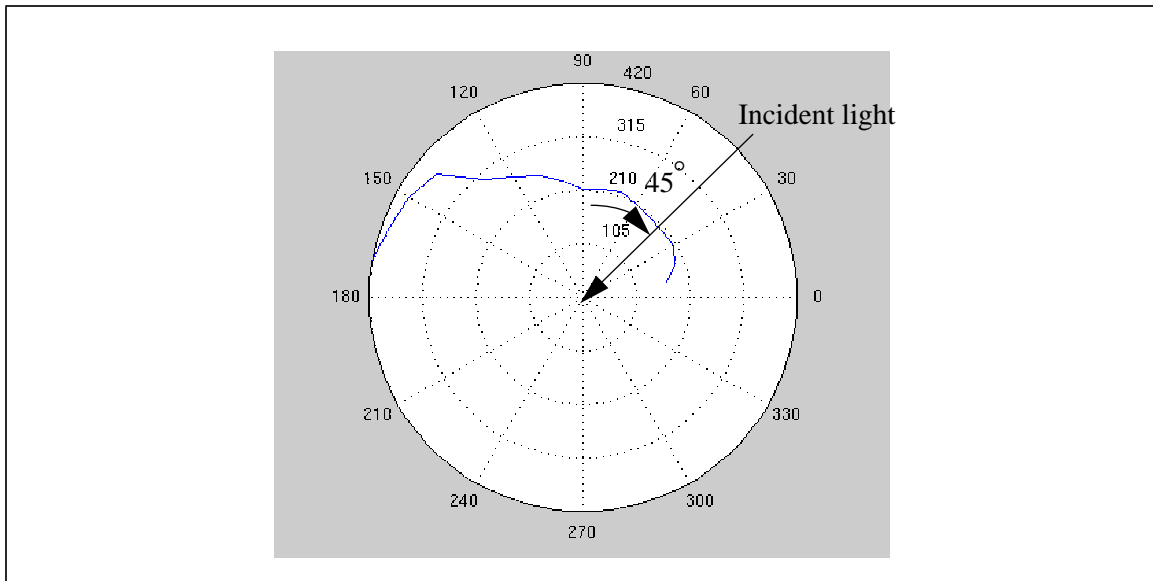


Figure 6.14 The incident plane of white paper's BRDFs with the incident direction at 45° to the right

6.2.2 Sample 2: Silk

From the result of the isotropic check of silk, we know it is anisotropic. In the following experiments, we take $\varphi_i = 180^\circ$ and 90° . Figure 6.15 to Figure 6.17 show the BRDFs for an incident light at $\varphi_i = 180^\circ$ and $\theta_i = 65^\circ$. Figure 6.18 to Figure 6.20 show the BRDFs for $\varphi_i = 180^\circ$ and $\theta_i = 45^\circ$. Figure 6.21 to Figure 6.23 show the BRDFs of $\varphi_i = 90^\circ$, $\theta_i = 65^\circ$. The view points (azimuth, elevation) are at $(-45^\circ, 50^\circ)$ in the side view figures and $(0^\circ, 90^\circ)$ in the overhead view figures.

It can be seen from the figures that silk reflects light strongly in directions close to its surface tangent, and the reflectance is very weak in directions close to incident direction. Compared to the photocopy paper, the reflective pattern of silk is not symmetrical

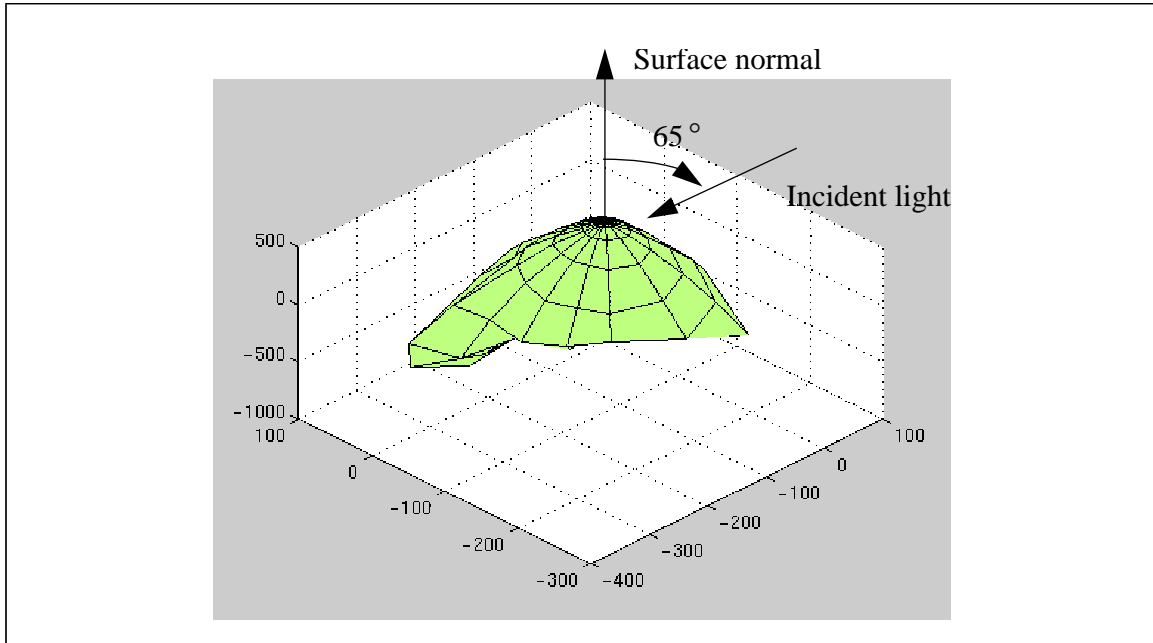


Figure 6.15 Side view of red silk's BRDFs with the incident direction at $(180^\circ, 65^\circ)$

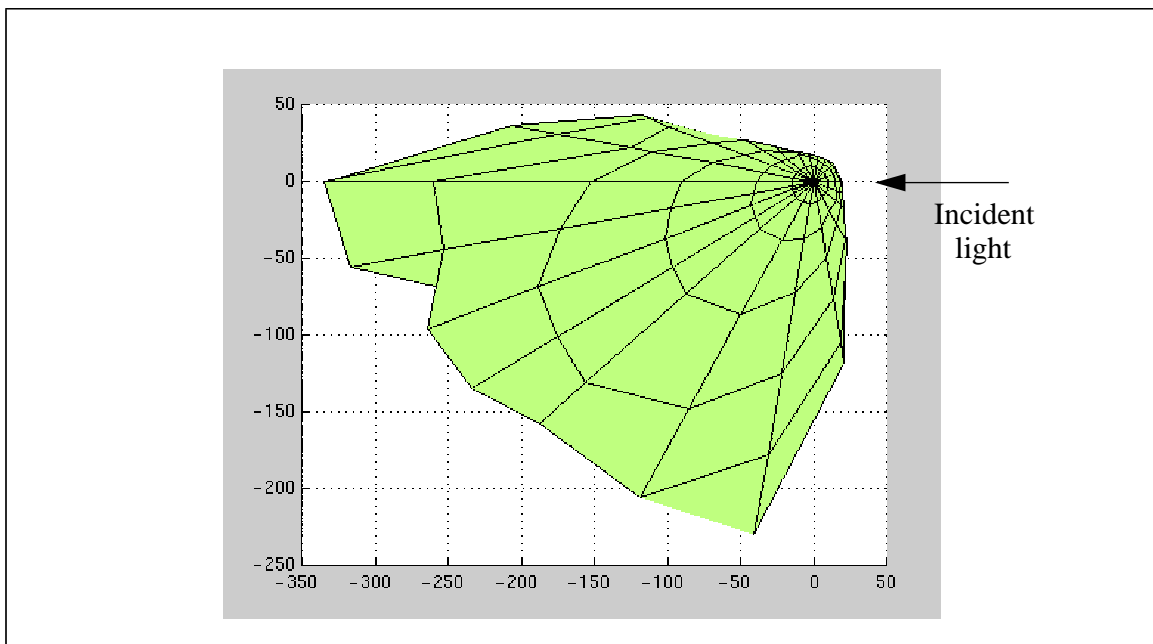


Figure 6.16 Overhead view of red silk's BRDFs with the incident direction at $(180^\circ, 65^\circ)$

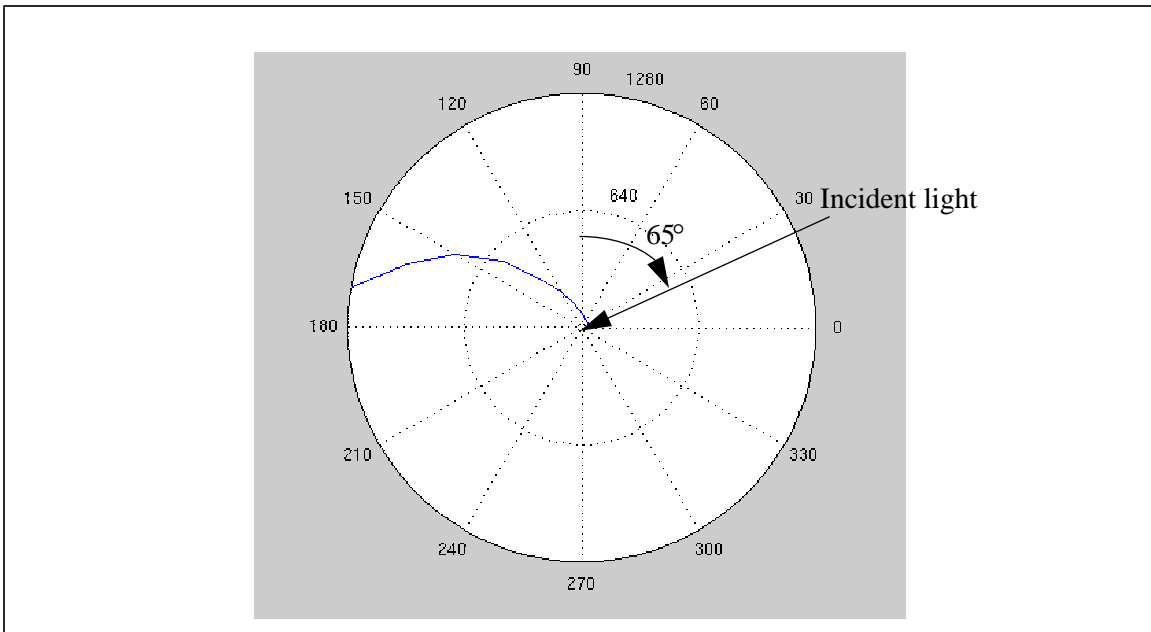


Figure 6.17 The incident plane of red silk's BRDFs with the incident direction at $(180^\circ, 65^\circ)$

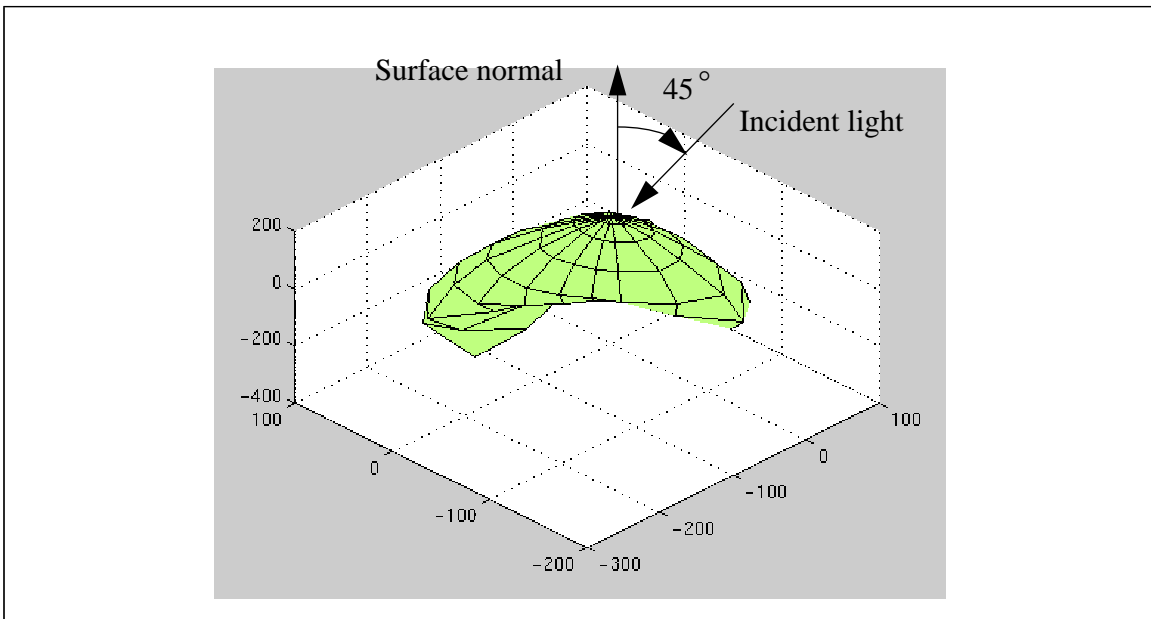


Figure 6.18 Side view of red silk's BRDFs with the incident direction at $(180^\circ, 45^\circ)$

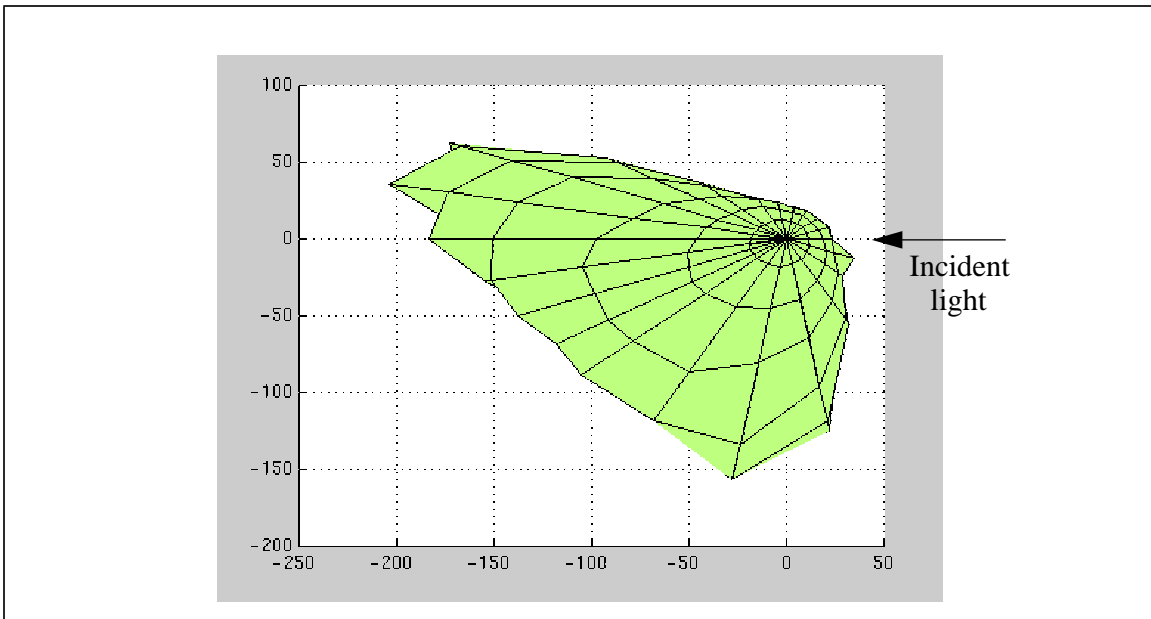


Figure 6.19 Overhead view of red silk's BRDFs with the incident direction at $(180^\circ, 45^\circ)$

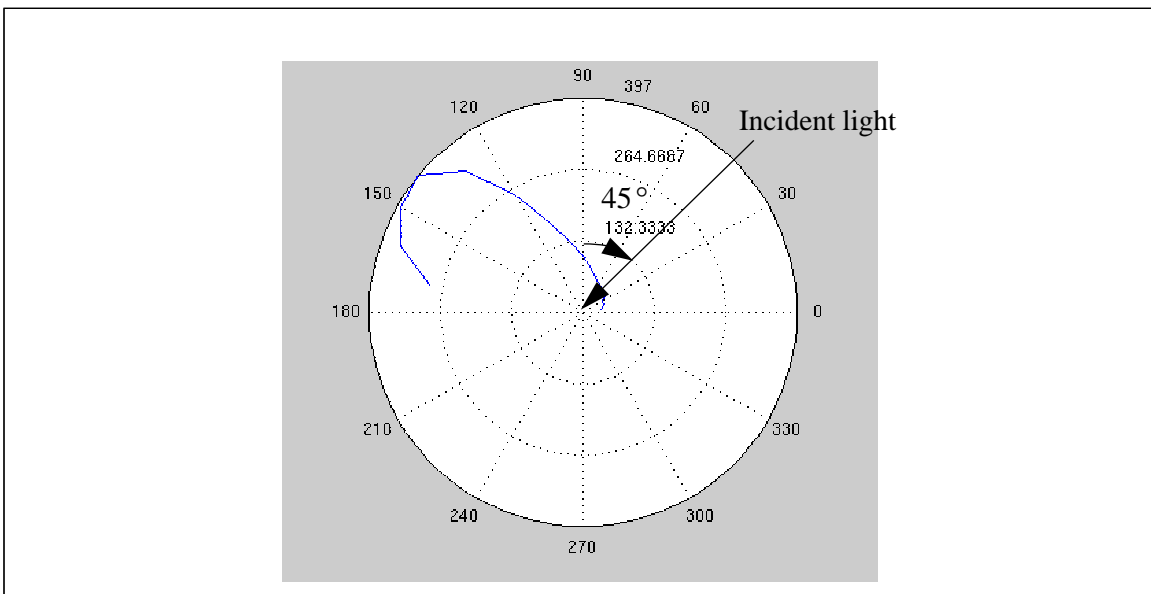


Figure 6.20 The incident plane of red silk's BRDFs with the incident direction at $(180^\circ, 45^\circ)$

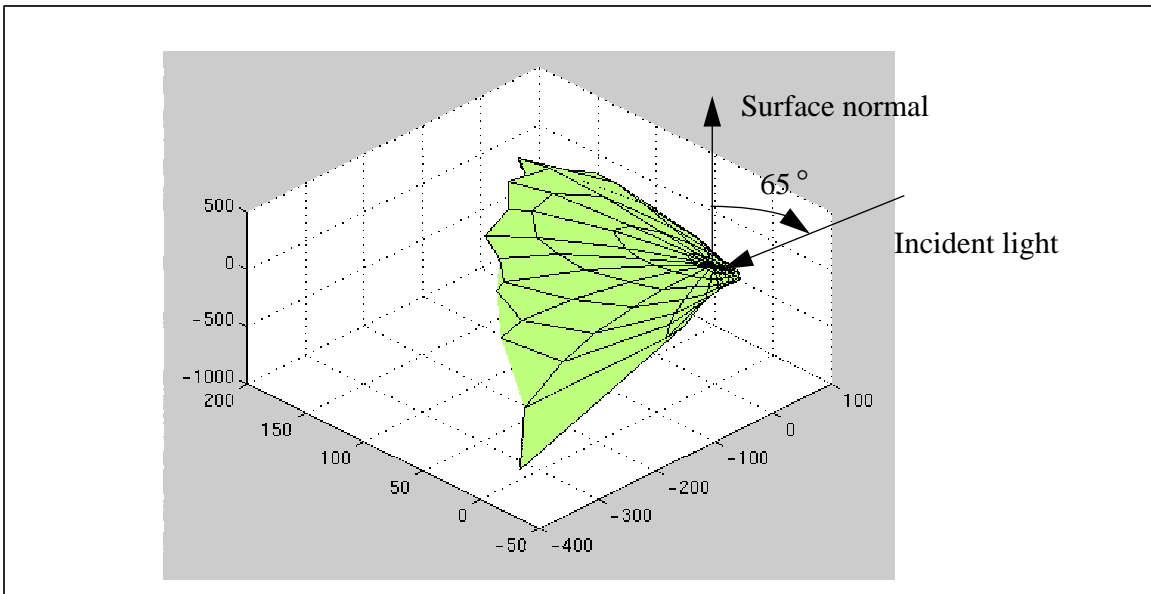


Figure 6.21 Side view of red silk's BRDFs with the incident direction at $(90^\circ, 65^\circ)$

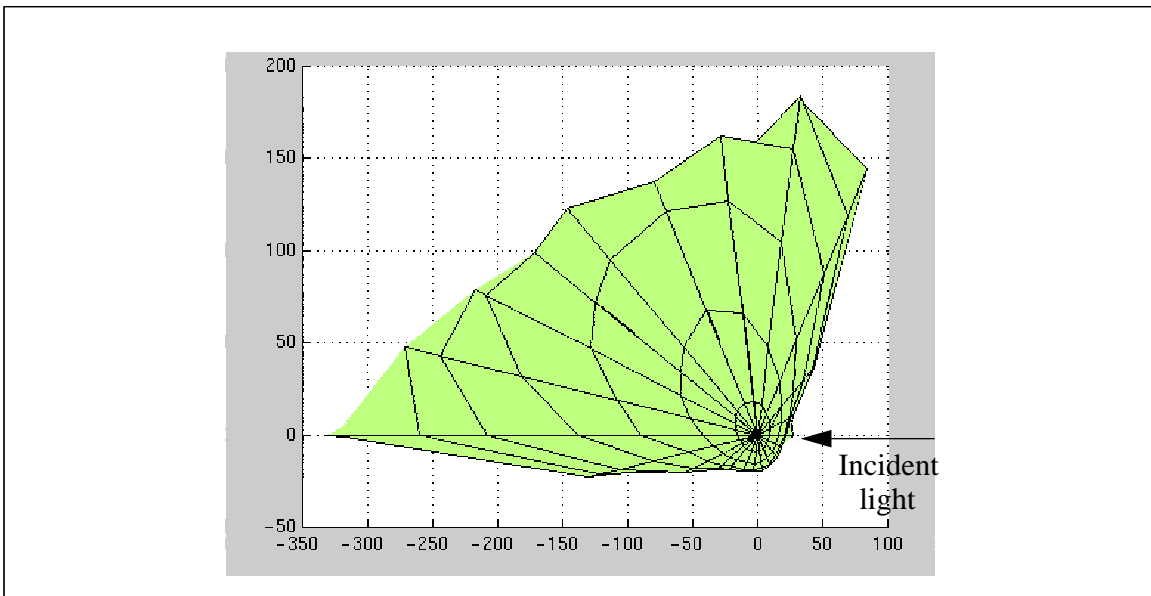


Figure 6.22 Overhead view of red silk's BRDFs with the incident direction at $(90^\circ, 65^\circ)$

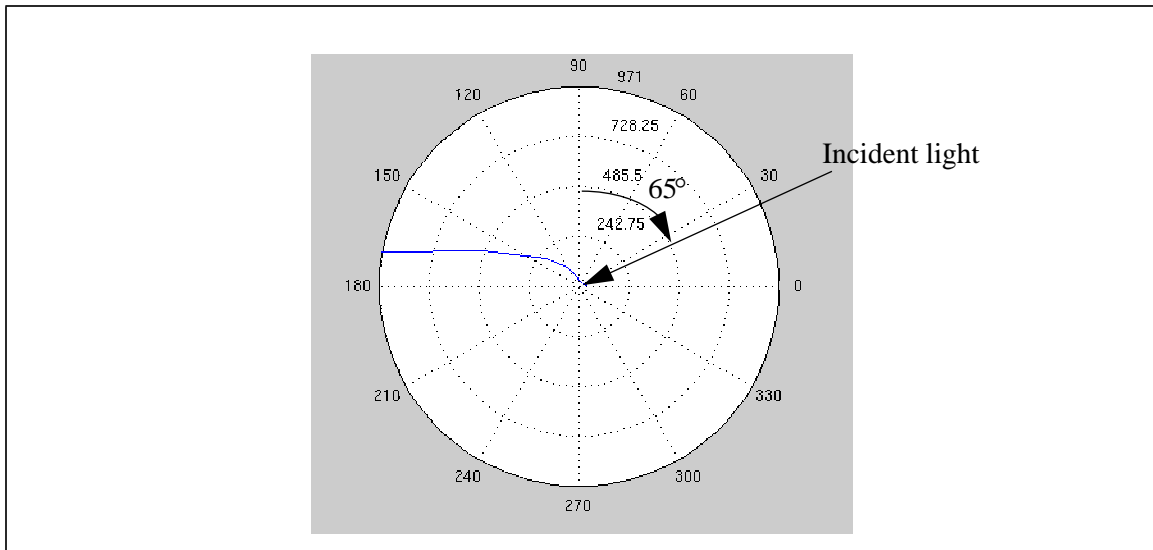


Figure 6.23 The incident plane of red silk's BRDFs with the incident direction at $(90^\circ, 65^\circ)$

6.3 Error Analysis

There are several factors that introduce errors in the experiments. These include:

- The variance of the light source intensity over time. Since images from different point of view are not taken at the same time, the incident light intensity may change over time due to the electric voltage change on the bulb. To find out how much error would be introduced by this cause, images were taken at different times while all other conditions unchanged. The average pixel value varies within ± 2 among images. Compared to the halfway of 0-255, this error is less than 2%. This is also a determination of the reproducibility of our measurements.
- Motion errors of test station and gantry. The rotation error of the test station is 10 arc-min (0.6°) [ACME], and the error introduced to the reflected angles by the gantry motor is less than 1° . Compared to their rotation range, $0^\circ - 360^\circ$ in azimuth and $0^\circ - 90^\circ$ in elevation, The overall error due to motion of test station and gantry is less than 2%.
- The standardizing process of pixel values. Although we calibrated the camera, and used the results to convert the pixels values with different camera parameters, the calibration itself has errors in it. If we change both the shutter-speed and the f-number during the experiment, the over all error is within 5% (see Section 4.2). If we change only the shutter-speed, the error is

within 2%. In the data given in this chapter, only shutter-speed has been changed during the experiment.

- Light coming from sources other than the designated light source. During the experiment, the designated light source should be the only light source for the sample. This can be achieved by turning off all other lights in the room. The difference in pixel values between turning all room lights off and leaving one room light on (which is far away from the sample and cannot illuminate the sample directly) is 1 to 2. Thus creates an error of 1-2% compared to the halfway of 0-255. Moreover, it is a constant systematic error and can be corrected by subtracting each pixel value by 1-2. In our experiment, one room light is on and it is far away from the sample.

Given our experimental conditions, the overall error in our experiment is less than 8% in the worst case for the standard pixel value. This satisfies the requirement of “rough reflectance property” for image synthesis, since what really counts there are the relative values of the BRDF.

Chapter 7

Conclusion and Future Work

7.1 Conclusion

Using the ACtive Measurement Facility (ACME) as a basis, we built and used an automated BRDF measurement system whose results can be used for image synthesis in computer graphics. A 3-channel CCD camera was calibrated as a function of the incoming light irradiance, the camera's f-number and the camera's shutter speed. A set of computer controlled motion platforms, including a test station of three degrees of freedom and a gantry with five degrees of freedom, were used to give the whole system enough degrees of freedom to carry out BRDF measurement. Using this system, the partial BRDF of several materials were measured with an overall error of less than 8%. The whole system is programmed in Java and will be soon accessible from the Internet. We have shown that such a system is viable and convenient to determine BRDF of materials of interest in image synthesis.

7.2 Future Work

Our system can be improved in several ways with respect to the automation process and the accuracy of measurement.

7.2.1 Improvement of Accuracy

The measuring device is a 3-channel 8-bit CCD camera, which has only 0-255 range on each RGB channel. If the output range can be increased to 0-4096, which means a 12-bit camera, camera settings do not need to be changed extensively during the experiment and

therefore the measurement process will be faster and results will be more accurate.

Our camera is only calibrated at one set of fixed camera parameters. For example, the calibration of pixel values vs. radiometer readings is done only for f-stop =120 and shutter speed = 100 (see Chapter 4). It is possible that the two parameters have effect to each other, which means that they are not independent to each other. In that case, more calibration could be done for different camera parameter settings. Also, the average of the three channels of RGB were used in our calibration. More specific calibrations can be done on each channel. This will help the data conversion to be more precise.

7.2.2 Automating the Whole Process

In the system we constructed so far, the light source is not movable. It was either attached to the test station or to the test bed. Under this configuration, the process is only automated in changing incident azimuth angle φ_i (by rotating the test station), reflected azimuth angle φ_r and reflected elevation angle θ_r (by moving the gantry). The incident elevation angle θ_i has to be changed by adjusting the position of the light source manually. This is why we were only able to measure partial BRDFs with a very limited number of incident directions. One possible way to automate the control of θ_i is to hold the light source with a robot arm. A robot arm is available in LCI [Pai99], however, it cannot in its current configuration hold the light source. Some changes have to be made before it can be used in this way.

7.2.3 BRDF Verification

While we obtained reliable data by using our automated BRDF measuring system, we did not verify our data experimentally. One possible way to verify the data is using the system to measure some materials with known models of BRDFs. The most accessible materials of this kind are almost perfectly diffuse (Lambertian) materials, such as chalk or some pottery. In this case, the ideal BRDF is a constant in all directions. If the measurement results are approximately the same as their known BRDFs, the measurement result can be trusted. Another way to verify the data is to measure some materials that had been already measured in other labora-

tories, and compare our data with theirs.

Bibliography

- [Blin77] James F. Blinn. Models of Light Reflection For Computer Synthesized Pictures. SIGGRAPH'77 Proceedings, Vol.11, No.2, pp.192-198, July 1977.
- [Cohen93] Michael F. Cohen and John R. Wallace. Radiosity and Realistic Image Synthesis. Academic Press Professional, 1993.
- [Cook82] R.L. Cook and K.E. Torrance. A Reflectance Model for Computer Graphics. ACM Transactions on Graphics, Vol.1, No.1, pp.7-24, January 1982.
- [Dana96] Kristin J. Dana, Shree K. Nayar, Bram van Ginneken and Jan J. Koenderink. Reflectance and Texture of Real-World Surfaces. Columbia University Technical Report, CUCS-048-96, December 1996.
- [DeYoung97] Joel M. DeYoung and Alain Fournier. Properties of Tabulated Bidirectional Reflectance Distribution Functions. Graphics'97 Proceedings, pp. 47-55, May 1997.
- [Fournier96] Alain Fournier. Computer Graphics: Light, Vision and Colour. Course Notes, Department of Computer Science, University of British Columbia.
- [Germer97] T.A. Germer and C.C. Asmail. A goniometric optical scatter instrument for bidirectional reflectance distribution function measurements with out-of-plane and polarimetry capabilities. Scattering and Surface Roughness, ed.Z.-H. Gu and A.A. Maradudin, SPIE Proceedings 3141, pp.220-231, 1997.

-
- [He91] Xiao D. He, Kenneth E. Torrance, Francois X. Sillion and Donald P. Greenberg. A Comprehensive physical model for light reflection. SIGGRAPH'91 Proceedings, Vol.25, No.4, pp.175-186, July 1991.
- [Horn79] Horn, B.K.P. and Sjoberg, R.W. Calculating the Reflectance Map. Applied Optics, 18:1770-1779, 1979.
- [IL1700] General Instructions, IL1700 Research Radiometer/Photometer. International Light Inc, 1998. <http://www.intl-light.com/manuals/index.html>
- [Karner96] Konrad F. Karner, Heinz Mayer and Michael Gervautz. An Image based Measurement System for Anisotropic Reflection, EUROGRAPHICS, Vol.15, No.3, pp.119-128, August 1996.
- [LMH] Alex Ryer. Light Measurement Handbook. International Light Inc, 1998. <http://www.intl-light.com/handbook/index.html>
- [Pai99] D. K. Pai, J. Lang, J. E. Lloyd and R.J. Woodham. ACME, A Telerobotic Active Measurement Facility. 6th International Symposium on Experimental Robotics, Sydney, Australia, March 1999.
- [PCG-96-1] Steve S-F. Chen, Jerry Wei-Chieh Li, Kenneth E. Torrance, Sumanta N. Pattanaik. Preliminary Calibration of the Photometrics PXL1300L CCD Camera. Technical report, no. PCG-96-1, Program of Computer Graphics, Cornell University, 1996.
- [PCG-98-1] Sumanta N. Pattanaik and Kenneth E. Torrance. Light Measurement using the Photometrics-PXL1300L CCD Camera. Technical report, no. PCG-98-1, Program of Computer Graphics, Cornell University, 1998.
- [Phon75] Bui-T. Phong. Illumination for Computer Generated Pictures. Communications of the ACM, Vol.18, No.6, pp.311-317, June 1975.
- [Poul90] Pierre Poulin and Alain Fournier. A model for anisotropic reflection. SIG-
-

-
- GRAPH'90 proceedings, pp.273-281, August 1990.
- [Murray90] J.F. Murray-Coleman and A.M. Smith. The Automated Measurement of BRDFs and their Application to Luminaire Modeling. Journal of the Illuminating Engineering Society, pp. 87-99, Winter 1990.
- [Nico77] F.E. Nicodemus, J.C. Richmond, J.J. Hsia and I.W.Ginsberg. Geometrical Considerations and Nomenclature for Reflectance. National Bureau of Standards (US), October 1977.
- [RCCL] John Lloyd and Vincent Hayward. RCCL/RCI System Overview. McGill Research Centre for Intelligent Machines, McGill University, July 1992.
- [Robot93] Robert R. Lewis. Making Shaders More Physically Plausible. Fourth EUROGRAPHICS Workshop on Rendering, pp. 47-61, June 1993.
- [Sing97] Sing Choong Foo. A Gonioreflectometer for Measuring the Bidirectional Reflectance of Material for Use in Illumination Computation. Master's Thesis, Cornell University, August 1997.
- [Sony950] 3-CCD Color Video Camera DXC-950 Sales Manual. Sony Cooperation.
- [Torr67] K.E. Torrance and E.M. Sparrow. Theory for Off-Specular Reflection from Roughened Surfaces". Journal of Optical Society of America, Vol.57, No.9, 1967.
- [Ward92] Gregory J. Ward. Measuring and Modeling Anisotropic Reflection. SIG-GRAPH'92 proceedings, pp. 265-272, July 1992.
- [Wysz82] G. Wyszecki and W.S. Stiles. Color Science: Concepts and Methods. Quantitative Data and Formulae, Wiley, 1982.

Appendix A

Light Measurement Basics

A.1 Light Basics

Light is one portion of the various electromagnetic waves. Visible light is just a narrow band of it.

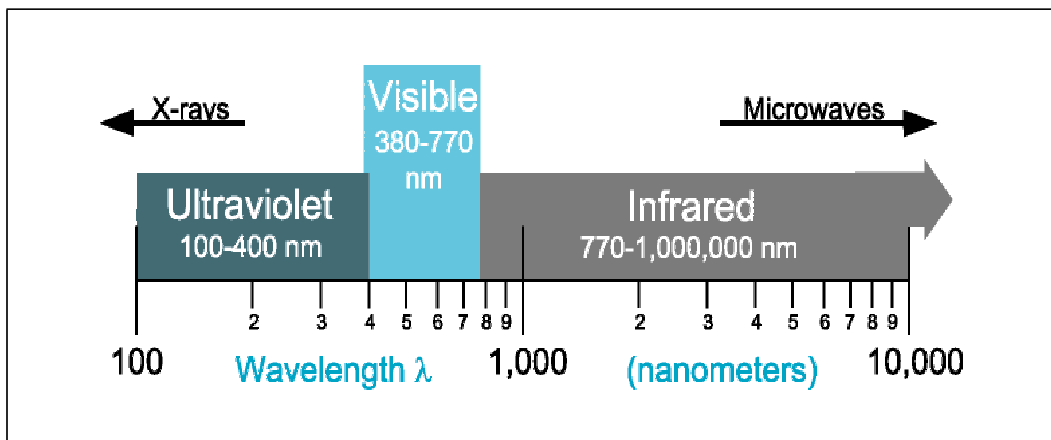


Figure A.1 The optical portion of the electromagnetic spectrum (copied from [LMH])

Even within the visible light range, the response of the human eye varies as a function of the wavelength. Yellow-green light has the greatest weight because it stimulates the eye more than blue or red light of equal radiometric power. The CIE 1931 Standard Observer established a standard based on the average human eye response under normal illumination. The tristimulus curve $\bar{y}(\lambda)$ graphed in Figure A.2 is the CIE $V(\lambda)$ function, which represents the sensitivity of human eye to different wavelength. For more information about color theory refer to [Wysz82].

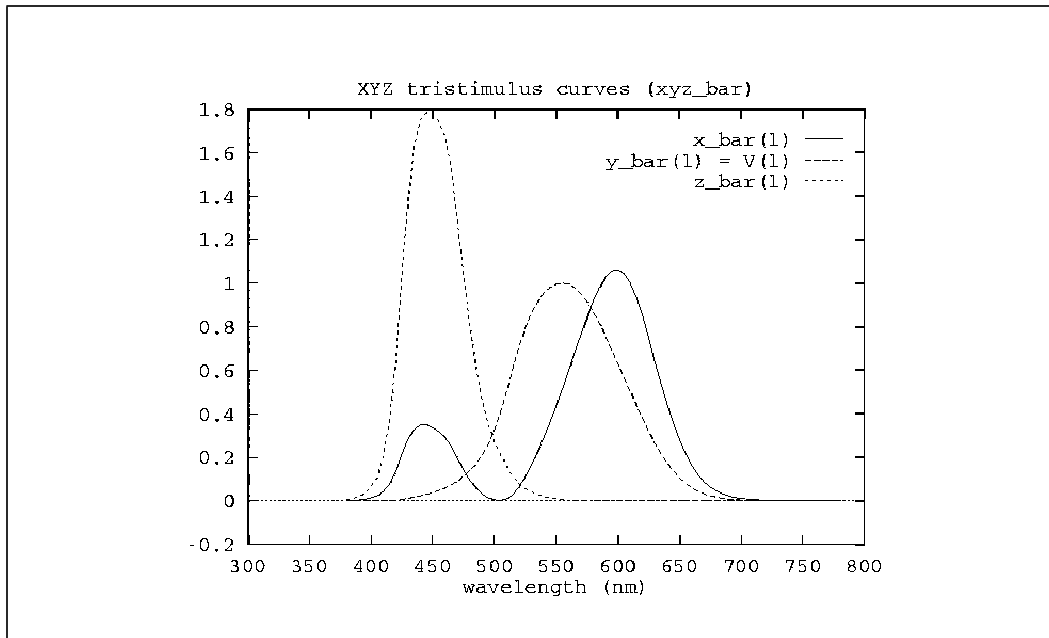


Figure A.2 CIE spectral tristimulus curve (copied from [Fournier96])

A.2 Measurement Principles

A.2.1 The Inverse Square Law

Assume there is no absorption in the space, the inverse square law states that for a point light source, the intensity per unit area varies in inverse proportion to the square distance to the light source. In other words, if 16 W/cm^2 is measured at 1 meter, 4 W/cm^2 will be measured at 2 meters, and the irradiance at any other distance can be calculated by

$$E_1 d_1^2 = E_2 d_2^2 \quad (\text{Eqn A-1})$$

A.2.2 Lambert's Cosine Law

The *cosine law* states that the irradiance or illuminance (see Section A.3 for definition) falling on any surface varies as the cosine of the incident angle θ ,

$$E_\theta = E \times \cos \theta \quad (\text{Eqn A-2})$$

The perceived measurement is orthogonal to the incident flux and is reduced at oblique angles, causing light to spread out over a wider area than it would if perpendicular to the measurement

plane.

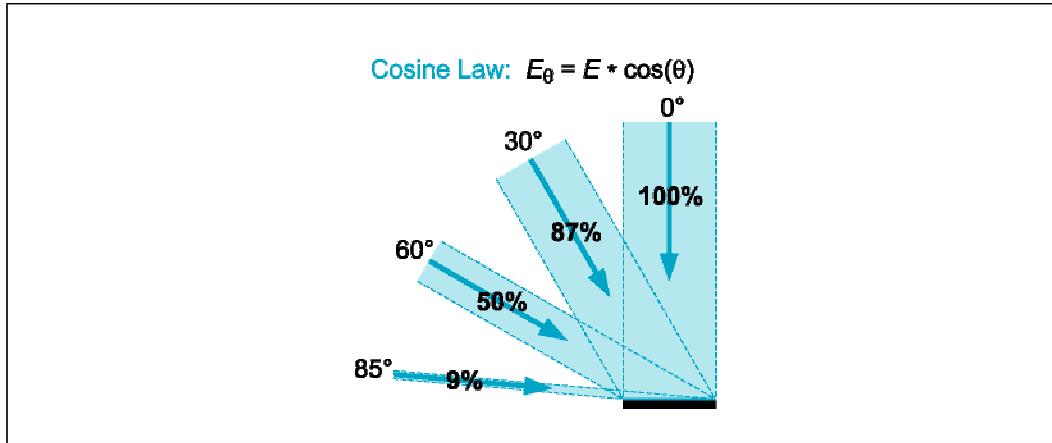


Figure A.3 Lambert's cosine law

A.3 Related Units

In most graphics systems, optical quantities are simply denoted by red, green and blue triplets. While in physics, or in most light measuring systems, they are radiant, radiance, irradiance and etc. The definition of these quantities are given in this section, and a summary is presented in Table A.1.

Table A.1 Radiometric quantities

Physics	Radiometry	Radiometric Units
Flux	Radiant power	watts [W = joules/second]
Flux	Luminous power	lumens [talbots/second]
Flux density	Irradiance	[W/m ²]
Flux density	Illuminance	lux [lumens/m ² /sr]
Angular flux density	Radiance	[W/cm ² /sr]

Radiant flux is a measure of radiometric power. Flux, expressed in watts, is a measure of the rate of energy flow, in joules per second. *Luminous flux* is a measure of the power of visible light. *Photopic flux*, expressed in lumens, is weighted to match the responsiveness of the human eye, which is most sensitive to yellow-green (see Figure A.2).

Irradiance is a measure of radiometric flux per unit area, or flux density. Irradiance is typically expressed in W/cm^2 (watts per square centimeter) or W/m^2 (watts per square meter). *Illuminance* is a measure of photometric flux per unit area, or visible flux density. Illuminance is typically expressed in lux (lumens per square meter) or foot-candles (lumens per square foot).

The unit of solid angle is *steradian*. A steradian is defined as the solid angle which, having its vertex at the center of the sphere, cuts off a spherical surface area equal to the square radius of the sphere.

$$\Omega = \frac{A}{R^2} \quad (\text{Eqn A-1})$$

Thus a sphere has 4π steradians.

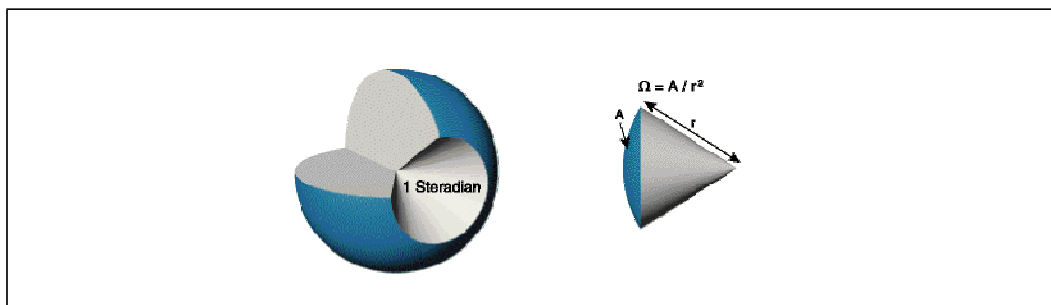


Figure A.4 Steradian, unit of solid angle

Radiance is a measure of the flux density per unit solid angle (or steradian), expressed in $\text{W}/\text{cm}^2/\text{sr}$ (watts per square centimeter per steradian) or $\text{W}/\text{m}^2/\text{sr}$ (watts per square meter per steradian). For a point light source, radiance is independent of distance as opposed to irradiance. Because the area a solid angle covers becomes larger as the distance further.

Appendix B

Operating Procedures and Precautions

Measuring a BRDF involves huge amounts of data. With the ACME facility and programming environment, this process is automated. The steps to set up the experiment are given in this section.

B.1 Camera Calibration

Camera calibration is needed only when some critical camera settings are changed or a different camera is used in the experiment (refer to camera's manual). The camera is calibrated for different parameters (see Chapter 4). The linear response calibration uses a radiometer's reading as comparison to the camera's pixel value. Before the calibration, read the manual of the camera ([Sony950] in our case), general instructions of the radiometer [IL1700], and the light measurement basics in *Light Measurement Handbook*[LMH].

There are three things important to be aware of,

1. When using a radiometer, the sample surface has to be at least as large as the barrel's front lens [LMH]. Zero the radiometer before using it.
2. Set all the switches on the side of camera to the "auto" position to allow the computer to control it. If using a different camera, refer to its manual.
3. As in the BRDF measurement, a linear response of the camera is desired. This requires to set the Gamma to be OFF, not ON.

B.2 Experiment Process

B.2.1 Hardware Side

ACME motion is controlled by a PC named *kiewa*, which runs SunOS5.6. There is a power switch for the amplifiers under *kiewa*. Before turning the power switch on, check the position of the gantry and make sure that the rotation of the pantilt head will not make the camera collide with something else. Now turn on the power. Notice that the pantilt head is reset to its original position when power is turned on.

Check if the motion controller card works correctly. Login to *kiewa*, and set the *RCCL* environment (see *RCCL* manual [RCCL]). Then we can use the *RCCL* commands to move the gantry and the test station. For example:

```
move gantry to 200 200 0
```

is to move the gantry to $x = 200\text{mm}$, $y = 200\text{mm}$ and $z = 0$.

If this works, the controller card works correctly. If not, we can reload the software into the controller card by

```
/ai/kingdon/acme/scripts/bootit
```

B.2.2 Software Side

Since ACME motion is controlled by the PC named *kiewa* and camera is controlled by the PC named *oly*, which runs Linux. Servers are needed to be run on *kiewa* to listen to the motion request from *oly*. A Remote Method Invocation registry process and two servers need to be running while doing the experiment:

```
rmiregistry&
```

```
java acme.RobotInfoServer&
```

java acme.RcclConnectionServer

If kiewa has been rebooted, a patch needs to be run as well:

/usr/local/bin/rtpatch

Now it is ready to run the experiment on *oly*, or on any authorized machine that can connect to *oly* via the internet. Don't forget to turn off the room lights before you start. and make sure your file system has enough space to save several hundreds of images.

Appendix C

Resources and their locations

The hardware resources include the sonyDXC-950 CCD camera, the IL1700 research radiometer, the parallel light source, the test station and the gantry. They are all in the Laboratory for Computational Intelligence(LCI) of Computer Science Department, UBC.

For the updated environment of ACME, refer to *file:/lci/project/acme/user/doc/index.html*. Different software versions can be checked out at */lci/project/acme/cvs*. The RCCL programming environment and relevant documents are located at */lci/project/rccl*. There are different version as well. The latest version when the thesis was written was RCCL5.0.